Chapter 4

Design of LNA analogues using combined Density Functional Theory and Molecular Dynamics approach for RNA therapeutics

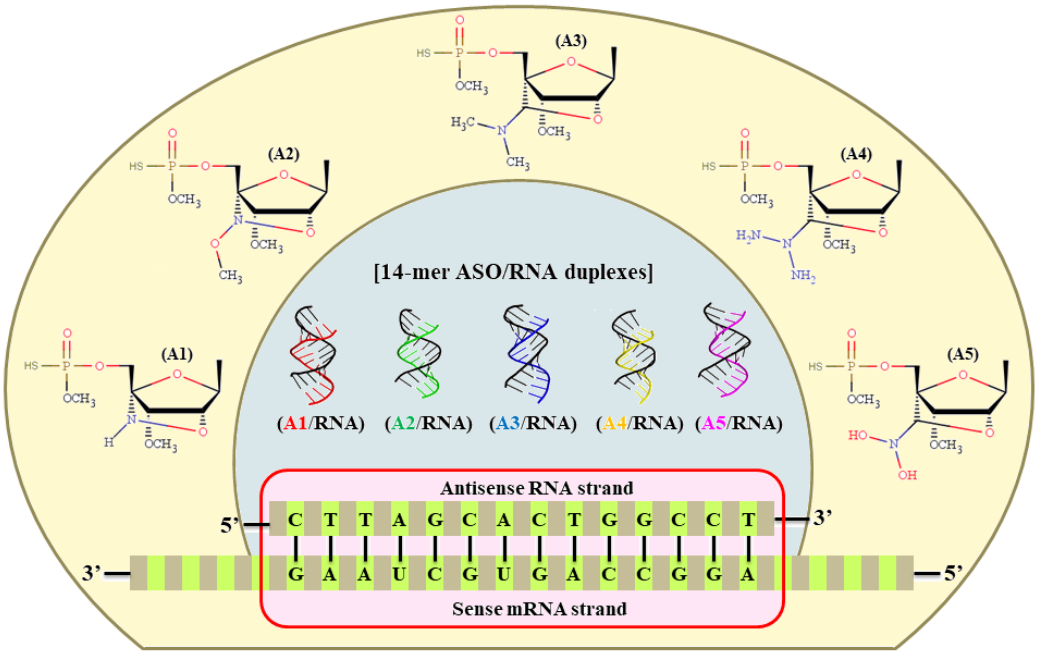

4.1. Introduction

Using antisense-mRNA as a medicine is a fundamentally different approach compared to treating diseases using traditional pharmaceuticals [1-3]. mRNA contains the set of instructions which direct cells in the human body to make proteins. Life depends on these proteins as every function in the human body both normal and disease-related, is carried out by one or many proteins in coordination. Human diseases are majorly the result of inappropriate protein production or disordered protein performance. Antisense-mRNA based drugs, designed to bind sequence specifically to their target mRNAs inhibit the production of diseases causing proteins and modulate their gene expressions. Unlike the small drug molecules and monoclonal antibodies, these synthetic antisense drugs are complementary to their sense-mRNAs which take advantage of normal biological processes to suppress the production of disease-causing proteins and create a desired therapeutic effect [4-6].

Antisense medications are chemically modified antisense oligonucleotides (ASOs/AONs) complementary to their target mRNAs, bind by *Watson-Crick* base pairing forming ASO/RNA hybrid duplexes. mRNA bound by an ASO activates the cellular endonuclease RNase H which further cleaves the RNA strand selectively from the ASO/RNA hybrid duplexes [7-8]. However, due to confined stability in biological media, the ASOs undergo rapid degradation even before duplexing and thus to protect and enhance their binding affinity and cellular uptake, the existing ASOs need to undergo chemical modifications to impart a valid antisense response. In the early stages, the phosphodiester backbones of the nucleotides were modified by replacing one of the non-bridging oxygen atoms by sulphur [9-10]. Briefly categorized under first generation ASOs, methylphosphonates and phosphoramidates gained significant attention, yet phosphorothioates were the most successful to induce the RNase H functions [11-13]. The first antisense drug marketed under the brand name “Vitravene” (ISIS-2922) approved by FDA in 1998 was a PS-oligonucleotide prescribed for the treatment of cytomegalovirus induced retinitis. However, in some cases, specificity, binding affinity to the target sequences and cellular uptake profiles of the PSs were less satisfactory. Hence, the drawbacks of the first-generation antisense modifications were compensated by the second-generation antisense modifications where the 2′-hydroxyl group of the furanose sugar ring was considered to further improve the pharmacokinetics of the ASOs. The 2′-O-methyl (OMe) and 2′-O-methoxyethyl (MOE) are the most well

explored second generation antisense modifications reported to be less toxic with enhanced binding affinity [14-15]. To extract outmost benefit, these sugar-based modifications were combined with the PS backbone linkage to generate chimeric ASOs which could resolve the problem of nuclease resistance and also target binding affinity. Many such antisense molecules are available in the market as FDA approved drugs, where both PS and MOE modified ASOs are used to generate chimeric ASOs [16-19]. Several antisense drugs *Fomivirsen, Mipomersen, Eteplirsen, Nusinersen* etc. have been already approved by the FDA for treating cancer, cardiovascular diseases, and various infectious and inflammatory disorders [20-28]. Third generation antisense modifications, such as peptide nucleic acids (PNAs), locked nucleic acids (LNAs), bridged nucleic acids (BNAs), Morpholino oligonucleotides *etc.* were developed with the intention of obtaining better antisense modifications compared to the PS's and MOE's [29-32]. LNAs are locked by a methylene bridge connecting the 2′-oxygen with the 4′-carbon of the furanose sugar ring and are reported to be the most promising third generation antisense modification. Experimental studies carried out by medicinal chemists using LNA ASOs showed increased thermodynamic stability, nucleic acid recognition, aqueous solubility, sequence selectivity, bio-stability and favourable hybridization kinetics compared to that of natural oligonucleotides [33-35]. However, these constructs couldn't activate the RNase H cleavage mechanism and some of its kinds were undergoing rapid degradation by nucleases, being hepatotoxic [36]. The potency of these ASOs was then improved by 3 to 5-fold ($ED_{50} \approx$ 2-5 mg/kg) without causing hepato-toxicity which was achieved by improving the structural components of MOEs and the LNAs [37-38]. Powerful LNA analogues like the BNAs are as a result of unceasing efforts to engineer the LNA structure. BNAs are hence structural extensions of LNAs developed to overcome the drawbacks of the LNA ASOs. Following a period of research and development, the 2′,4′-BNA^{NC} analogues: 2′,4′-BNA^{NC}[NH], 2′,4′-BNA^{NC}[NMe], N-Me-aminooxy BNA and N-MeO-amino BNA have been shown to be extremely promising in overcoming the drawbacks of LNA ASOs [39-40]. BNAs are significantly more nuclease resistant than the PSs and the LNAs in comparison. Studies on the BNA modifications conducted *in-vitro* and *in-vivo* revealed that when compared to MOE ASOs optimized BNA ASOs offered greater thermal stability, enhanced *in-vitro* activity and >5-fold improved *in-vivo* activity. Following this one can attempt to design novel antisense modifications to further improvise the antigene activity of existing LNA, BNA analogues.

Although there has been research on a few antisense modifications like cyclohexyl PNA, MOE *etc.* yet in-depth knowledge of the different antisense alterations now in use is severely lacking and must be obtained in order to create superior antisense modifications [41-47]. In chapter 3 we studied the structural and electronic properties of some existing LNA, BNA antisense modifications both at the monomer and oligomer level. The current study aims to design and understand the structural and functional significance of five novel LNA based antisense modifications labelled as A1, A2, A3, A4, A5 by establishing each with the five nucleic acids A, G, C, T, U respectively. Previously the modifications were designed considering the cytosine nucleobase only [47].

4.2. Materials and Methods

The complete methodology of the present work includes: First, Density Functional Theory (DFT) based quantum chemical study to obtain the most stable conformations of the monomer nucleotides containing the proposed LNA analogue antisense modifications (A1-A5) by establishing each with the five standard nucleobases Adenine (A), Guanine(G), Cytosine(C), Thymine(T) and Uracil(U) followed by derivation of quantum chemical descriptors for the same. Second, generation of force-field parameters of all the proposed modifications corresponding to the five nucleobases A,G,C,T,U followed by a detailed MD simulation study on a set of fully modified 14-mer ASO/RNA hybrid duplex systems targeting the protein PTEN mRNA nucleic acid sequence. Schematic 2D structures of the proposed LNA analogue antisense modifications (A1-A5) each containing nucleobases A, G, C, T, U respectively are given in Figure 4.1 and the modification details are listed in Table 4.1.

4.2.1. Density Functional Theory (DFT) Calculations

Starting structures of the modifications were built on the LNA monomer nucleotide structures using the Discovery Studio and Gauss View program package [48]. DFT based quantum chemical calculations were carried out to obtain optimized structures and ground state energies of all the monomer nucleotides using the Gaussian09 software package [49]. Full geometry optimization along with frequency calculations were done employing the meta-GGA, hybrid, unrestricted M06-2X functional alongside triple-ζ split valence and diffused basis set 6-311G(d,p) for all atoms, without imposing any symmetry constraints [50-53]. Using the conductor-like polarizable continuum solvation model (CPCM) water (with dielectric constant 78.39) was added as the solvent

implicitly [54]. Natural Bond Orbital (NBO) calculations were performed on the optimized structures at the same level of theory to generate wave function files. Molecular orbital composition analysis was carried out to find out the composition of the HOMO-LUMO iso-surfaces using the open source Multiwfn software program [55].

Table 4.1: Modification details of the proposed LNA analogue antisense modifications A1, A2, A3, A4, A5 each containing nucleobases Adenine (A), Guanine (G), Cytosine (C), Thymine (T) and Uracil (U), respectively along with the name codes used in the present work.

Modification Type	Name Code	Nucleobases	Modification Details
A1	A1-A	A-Adenine	2′-Oxygen and 4′-Carbon of the sugar moiety bridged by an N-linked LNA modification + PS backbone
	A1-G	G-Guanine	
	A1-C	C-Cytosine	
	A1-T	T-Thymine	
	A1-U	U-Uracil	
A2	A2-A	A-Adenine	2′-Oxygen and 4′-Carbon of the sugar moiety bridged by a Methoxy-N-linked LNA modification + PS backbone
	A2-G	G-Guanine	
	A2-C	C-Cytosine	
	A2-T	T-Thymine	
	A2-U	U-Uracil	
A3	A3-A	A-Adenine	2′-Oxygen and 4′-Carbon of the sugar moiety bridged by LNA linked to N-dimethyl modification + PS backbone
	A3-G	G-Guanine	
	A3-C	C-Cytosine	
	A3-T	T-Thymine	
	A3-U	U-Uracil	
A4	A4-A	A-Adenine	2′-Oxygen and 4′-Carbon of the sugar moiety bridged by LNA linked to N-diamine modification + PS backbone
	A4-G	G-Guanine	
	A4-C	C-Cytosine	
	A4-T	T-Thymine	
	A4-U	U-Uracil	
A5	A5-A	A-Adenine	2′-Oxygen and 4′-Carbon of the sugar moiety bridged by LNA linked to N-dihydroxy modification + PS backbone
	A5-G	G-Guanine	
	A5-C	C-Cytosine	
	A5-T	T-Thymine	
	A5-U	U-Uracil	

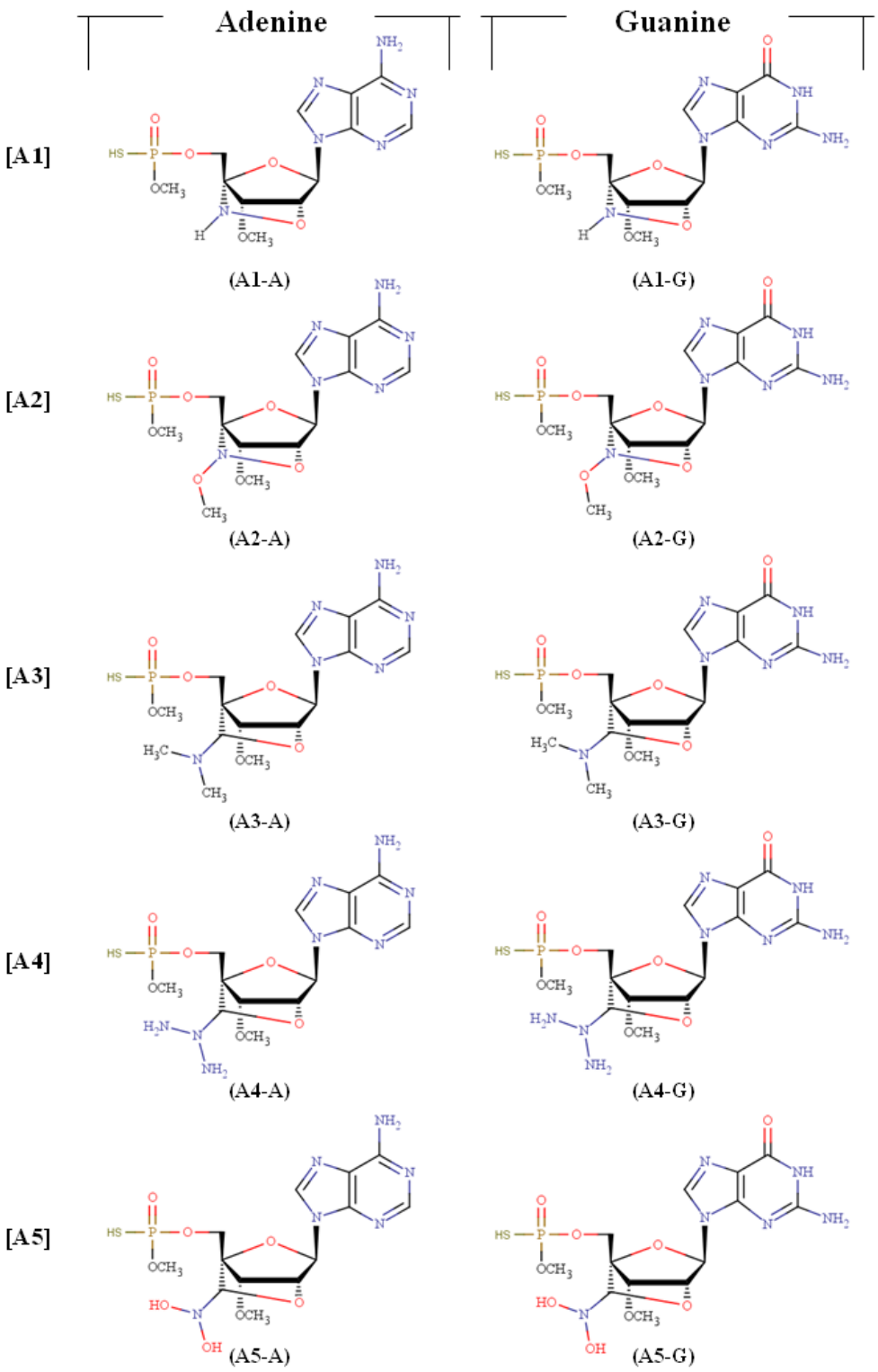

Figure 4.1: Schematic 2D representation of the proposed LNA analogue antisense modifications A1, A2, A3, A4, A5 each containing nucleobases Adenine(A), Guanine(G), Cytosine(C), Thymine(T) and Uracil(U), respectively.

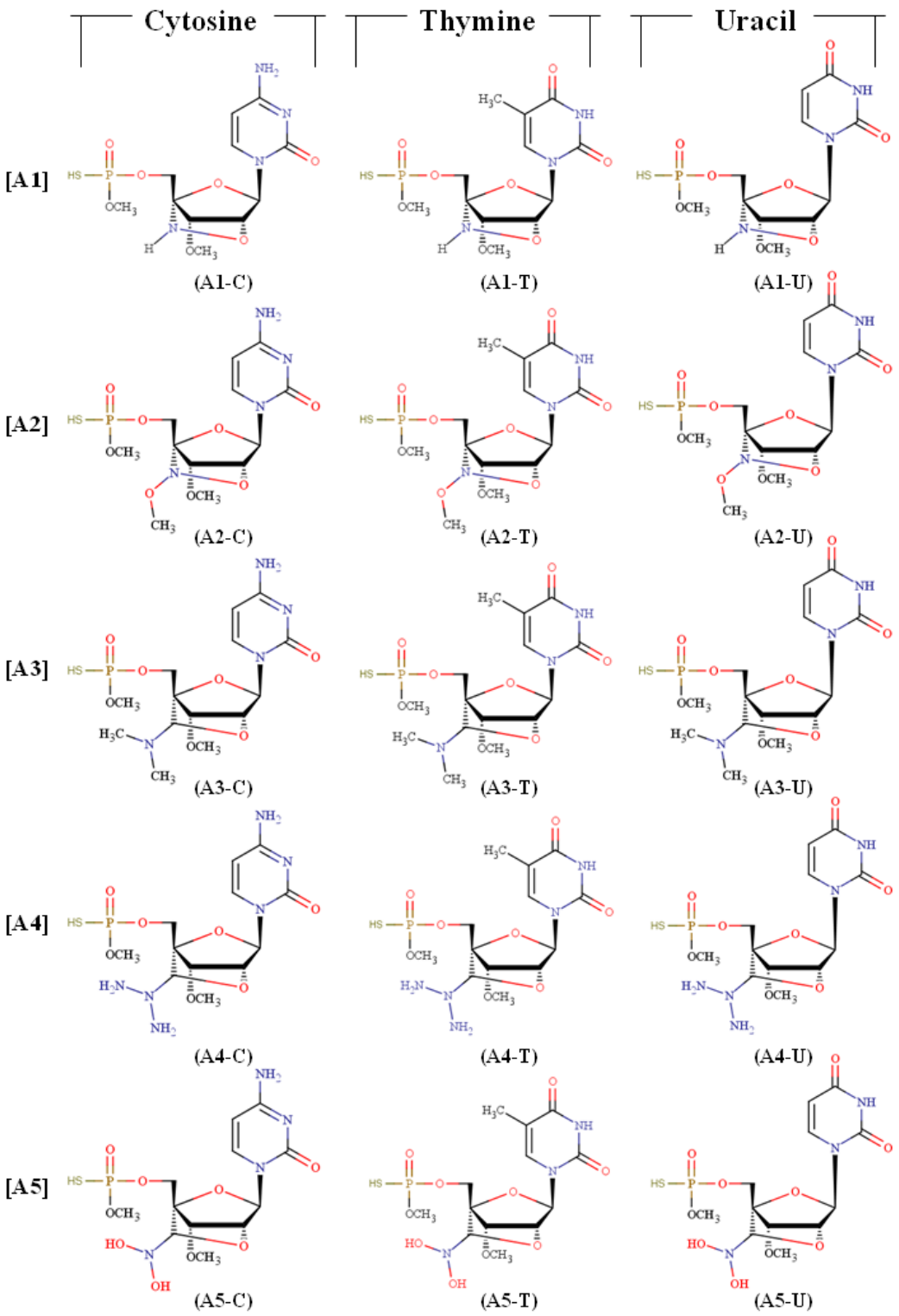

Figure 4.1: Schematic 2D representation of the proposed LNA analogue antisense modifications A1, A2, A3, A4, A5 each containing nucleobases Adenine(A), Guanine(G), Cytosine(C), Thymine(T) and Uracil(U), respectively.

4.2.1.1. Global reactivity descriptors

The *Koopmans'* theorem states that IP and EA values are the negative of energy eigen values as IP = $-E_{HOMO}$ and EA = $-E_{LUMO}$.

These fundamental equations are applied to the analysis of a set of global parameters that characterize the structural transitions between different ground states. Global reactivity descriptors global hardness (η), global softness (S), chemical potential (μ) and electrophilicity (ω) all were evaluated using the following equations as described below [56-58].

$$\text{Global hardness } (\eta) = (\text{IP} - \text{EA}) / 2$$

$$\text{Global softness (S)} = {}^{1}/_{2\eta}$$

$$\text{Chemical potential } (\mu) = -(\text{IP} + \text{EA}) / 2$$

$$\text{Electrophilicity } (\omega) = {}^{\mu^2}/_{2\eta}$$

4.2.2. Molecular Dynamics (MD) Simulations

4.2.2.1. System building and Force-field parameters

Force-field parameters were developed for the proposed antisense modifications (A1-A5) corresponding to the five nucleobases using the parameterization protocol given in literature [59-60]. Partial atomic charges were derived at the M06-2X/-311G** level of theory using the Gaussian09 program package [49]. RESP fitting was done using the ANTECHAMBER module of AMBER18 [61]. Post parameterization, a set of 14-mer ASO/RNA hybrid duplex systems composed of fully modified 14-mer (5′-CTTAGCACTGGCCT-3′) ASO strand containing the proposed modifications (A1-A5) and 14-mer (3′-GAAUCGUGACCGGA-5′) RNA strand as the target complementary sequence were built. Since the modifications are LNA based, a regular LNA/RNA hybrid has been considered as the control system for comparison. The systems were charge neutralized adding Na^+/Cl^- as counter ions and solvated explicitly with TIP3P water box [62]. The entire duplex building process was carried out using the leap module of AMBER implementing the standard force field parameters 'RNA.OL3' for RNA nucleobases and the in-house generated force-field parameters for the proposed antisense modifications [63-64].

4.2.2.2. Simulation Protocol and Trajectory Analysis

Simulations were carried out using the all-atom classical MD simulation framework of AMBER18. The systems were energy minimized using the steepest descent method for 5000 steps, followed by 5000 steps conjugate gradient method. Energy minimization was done using constraints of 100 kcal/mol initially and then gradually reducing the constraints on all the solute atoms. The systems were then heated slowly from 0 K to 300 K canonical ensemble by using constraints of 100 kcal/mol on all the solute atoms. Post heating, the systems underwent equilibration in an isothermal isobaric (NPT) ensemble in a similar way using constraints of 100 kcal/mol initially and gradually reducing the constraints on all the solute atoms. Simulations were performed under periodic boundary conditions by employing the *Particle Mesh Ewald* technique to account for the long-range electrostatics [65]. MD integration was carried out using a 2.0 fs time step, employing the SHAKE algorithm on all the bonds involving hydrogen atoms [66]. Langevin temperature equilibration scheme was used to maintain the system temperature. For non-bonding interactions, a cut-off distance of 10 Å was used. The systems were then allowed to simulate under production run conditions for 100 ns and the trajectories were used for analysis. The RMSD, RMSF, sugar pucker, N-glycosidic dihedral angles, inter-strand and intra-strand phosphate distances, H-bonds all were computed using the CPPTRAJ module of Amber Tools [67]. Solvent accessible surface area (SASA) was calculated for all the duplexes using the VMD program [68]. Base-pairing, Base-stacking and Helix-turning all were observed using the NASTRUCT module of AMBER. MMGBSA module of AMBER was used for calculating the free energy of the duplexes [69-70].

4.3. Results and Discussion

4.3.1. DFT Results

4.3.1.1. Structure and Energetics of the LNA analogue monomer nucleotides

LNAs are RNA derivatives in which a methylene bridge locks the 2′-oxygen with the 4′-carbon of the ribose sugar ring. The bridge causes a *C3′-endo* sugar puckering geometry which decreases the ribose's conformational flexibility and increases local organization of phosphate backbone. LNAs have stronger binding properties compared to MOE antisense modifications, but at the same time higher toxicity compared to the same [36]. In order to develop highly active ASO/mRNA therapeutic antisense candidates it is inevitable to enhance the potency and reduce probable toxicity of the

existing LNA ASOs. In the present study, we are proposing five novel LNA analogue antisense modifications A1, A2, A3, A4, A5 by establishing each with all the five standard nucleobases Adenine(A), Guanine(G), Cytosine(C), Thymine(T) and Uracil(U), respectively. The modifications are LNA based and have been designed considering the structural motifs of standard antisense modifications from the literature. In all the modifications, the 2′-oxygen and 4′-carbon of the ribose sugar ring are linked to each other by five different conformationally constrained functional groups, designed by infusing different oxy or nitro groups into the parent LNA structure. Keeping in mind the importance of nitrogen chemistry in natural nucleic acids, in modifications A1 and A2, the methylene bridge carbon of the LNA is replaced with nitrogen. In A2, an extra methoxy group is added to the bridged nitrogen. In A3, A4 and A5 N-dimethyl, N-diamine and N-dihydroxy groups were added to the LNA carbon of the methylene bridge, respectively. Methoxy motifs have been well established in 2′-oxygen sugar modifications and their incorporation has already proven to show better pharmacokinetic properties [19].

Metabolic stability and cellular uptake of modified ASOs are immensely improved by phosphorothioate (PS) modifications in coordination with sugar-based modifications. PS substitutions are known to immensely induce RNase H activity, serum stability and cellular uptake of modified ASOs and hence all the modifications were further impregnated involving the PS backbone linkage. Thus, the proposed modifications are designed in a way that they share the structural components of LNA, BNA, MOE and PSs along with other electronegative groups attached to the methylene bridge carbon of LNA. BNAs are structural extensions of LNAs developed to improve the drawbacks of existing LNA ASOs. The basic idea behind functionalizing the LNAs is to reduce the hepato-toxicity and enhance the overall pharmacokinetic properties of the LNA ASOs without disturbing the strong binding nature of LNAs.

LNA nucleotides are linked by similar phosphodiester linkages resembling the natural nucleic acids found in DNA, RNA with respect to adequate aqueous solubility and *Watson-Crick* mode of binding [71]. These similarities of LNA nucleotides compared to the DNA, RNA nucleotides attributes to the use of standard reagents and automated synthesizers, facilitating their handling and simplifying the experiments to synthesize them using conventional phosphoramidates chemistry. Also, mixing of DNA, RNA bases allow the affinity for complementary sequences or the susceptibility to

RNase H to be optimized for individual applications which further allows LNA-containing nucleotides to be interspersed among DNAs and RNAs [72].

However, to fine-tune the LNAs it is highly needful to have adequate information on the structure and electronic properties of the existing as well as the novel antisense proposals. Now, a molecular structure comprises of the distinctive elements that give rise to its physical, chemical, and biological capabilities, and a detailed quantum chemical study of the molecular geometries can aid in identifying the structure-activity link of related compounds. Herein, we report an elaborate study on the proposed antisense modifications both at the monomer and oligomer level. All the monomer nucleotides were subjected to a DFT based full geometry optimization followed by single point energy calculations on the optimized structures to evaluate their various structural and electronic properties at the monomer level. Optimized structures of the proposed LNA analogue antisense modifications (A1-A5) each containing nucleobases A, G, C, T, U calculated at the M06-2X/6-311G(d,p) level of theory are given in Figure 4.2.

To inhibit the production of disease-causing proteins, the synthetic ASOs should be able to bind to their target mRNAs, inhibit the protein synthesis and modulate their gene expressions. The methylene bridge of the ribose in LNAs constricts sugar puckering into the desired *C3'-endo* conformation, an important consideration for antisense therapeutic applications [73]. Also, the LNAs in complex with RNAs induce flanking RNA bases to adopt an *N-type* conformation which favors *C3'-endo* sugar puckering and activate RNase H cleavage of the bound RNAs. From the optimized structures it was observed that the sugar puckering criteria is fulfilled which showed no disturbance in the *N-type* conformation due to infusion of the proposed modifications.

Also, to bind sequence specifically to their target RNAs the modified LNA monomer nucleotides should exist in an *anti*-conformation, a property of *A-form* helix generally observed in RNAs. The chi (χ) torsion angle specifies the relative sugar-base orientation in standard nucleic acids. Chi (χ) values of all the modified nucleotides are listed in Table 4.2. In general, 'χ' falls into the range of +90° to +180°/ –90° to –180° (or 180° to 270°) corresponding to the *anti*-conformation in *A-form* nucleic acid duplexes [74]. From Table 4.2, 'χ' values of the modified LNA nucleotides suggest their relative sugar-base orientations to be in *anti*-conformation which can increase the strength of base pairing and base stacking interactions preferring for RNA-mimicking *A-form* helix during duplex formation.

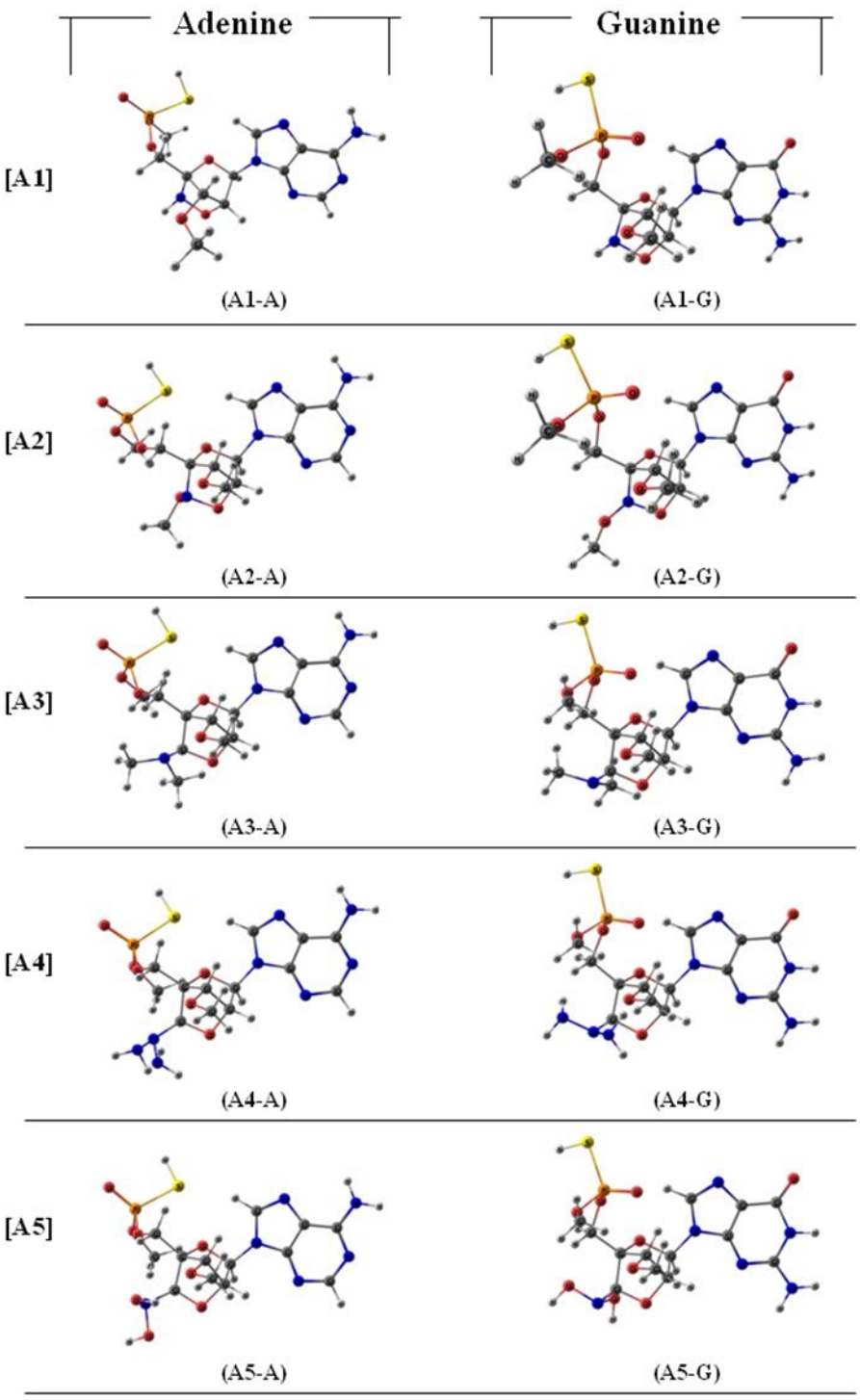

Figure 4.2: Optimized structures of the proposed LNA analogue antisense modifications A1, A2, A3, A4, A5 with their respective nucleobases Adenine(A), Guanine(G), Cytosine(C), Thymine(T) and Uracil(U) calculated at the M06-2X/6-311G(d,p) level of theory.

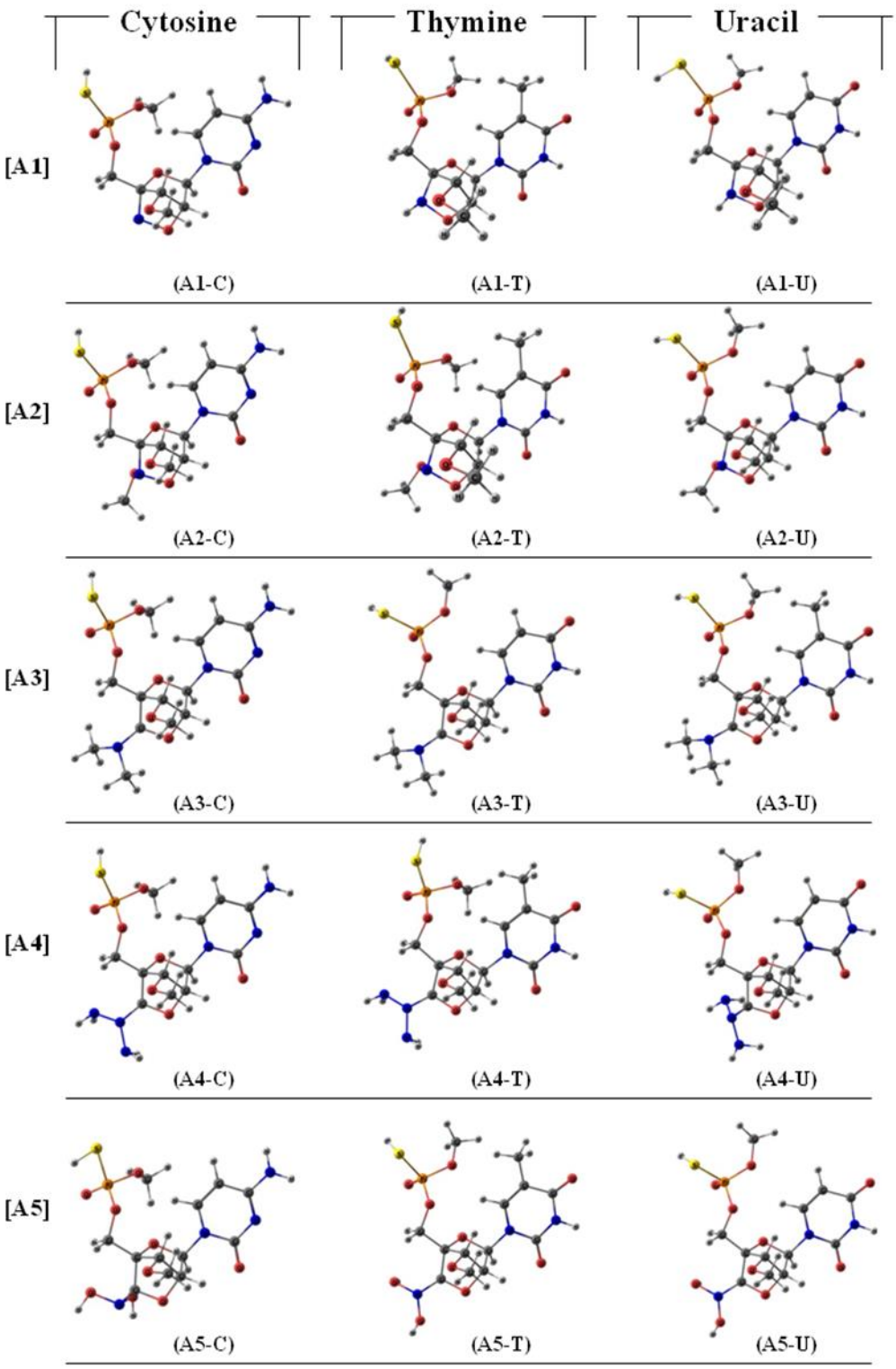

Figure 4.2: Optimized structures of the proposed LNA analogue antisense modifications A1, A2, A3, A4, A5 with their respective nucleobases Adenine(A), Guanine(G), Cytosine(C), Thymine(T) and Uracil(U) calculated at the M06-2X/6-311G(d,p) level of theory.

Table 4.2: The chi (χ) torsion angle, electronic energy, dipole moment, E_{HOMO}, E_{LUMO} and ΔE_{gap} of the proposed LNA analogue antisense modifications A1, A2, A3, A4, A5 with their respective nucleobases Adenine(A), Guanine(G), Cytosine(C), Thymine(T) and Uracil(U) calculated at the M06-2X/6-311G(d,p) level of theory.

Name Code	Chi (χ)	Electronic Energy (hartree)	Dipole Moment (D)	E_{HOMO} (eV)	E_{LUMO} (eV)	ΔE_{gap} (eV)
A1-A	-178.7	-1986.774755	5.90	-7.674	0.036	7.710
A1-G	-166.5	-2062.022488	9.71	-7.343	0.553	7.897
A1-C	-165.1	-1914.404476	9.86	-7.999	-0.134	7.865
A1-T	-164.9	-1973.596417	6.51	-7.996	-0.168	7.828
A1-U	-166.6	-1934.286304	6.21	-8.267	-0.259	8.008
A2-A	-176.8	-2101.239983	4.72	-7.682	0.028	7.710
A2-G	-169.7	-2176.485949	10.78	-7.352	0.541	7.893
A2-C	-165.8	-2028.871153	8.73	-8.034	-0.147	7.887
A2-T	-162.1	-2088.063050	2.57	-8.048	-0.226	7.821
A2-U	-167.5	-2048.751847	4.46	-8.290	-0.275	8.016
A3-A	-173.0	-2104.069445	4.86	-5.766	-0.109	5.658
A3-G	-167.8	-2179.314657	10.32	-6.005	-0.102	5.903
A3-C	-164.7	-2031.698037	7.35	-5.844	-0.245	5.599
A3-T	-163.9	-2090.889118	5.81	-5.879	-0.277	5.601
A3-U	-164.5	-2051.579474	6.64	-5.846	-0.297	5.549
A4-A	-173.4	-2136.108387	9.14	-6.617	-0.475	6.142
A4-G	-167.3	-2211.355947	9.75	-6.402	-0.194	6.208
A4-C	-164.5	-2063.741769	6.36	-6.108	-0.439	5.669
A4-T	-161.3	-2122.933761	2.88	-6.144	-0.474	5.670
A4-U	-166.9	-2083.619682	3.50	-6.253	-0.283	5.969
A5-A	-172.9	-2175.811314	8.48	-7.241	-0.788	6.453
A5-G	-165.5	-2251.060222	13.01	-7.000	-0.656	6.344
A5-C	-163.9	-2103.442453	5.87	-7.019	-0.690	6.329
A5-T	-164.0	-2162.632384	4.26	-6.848	-0.993	5.855
A5-U	-166.4	-2123.322541	4.94	-6.859	-0.988	5.871

4.3.1.2 Molecular Orbital analysis of the LNA analogue monomer nucleotides

The frontier molecular orbitals HOMO-LUMO are important quantum chemistry metrics which can reveal minute details about the accessible binding sites within the LNA analogue monomer nucleotides for interactions with the host molecules. The HOMO energy (E_{HOMO}), LUMO energy (E_{LUMO}), and the differences in their HOMO-LUMO energy gap (ΔE_{gap}) are therefore important indicators when taking into account the chemical reactivity and stability which can provide detailed information on the bonding nature of the monomer nucleotides. Calculated electronic energies, dipole moment, energies values of E_{HOMO}, E_{LUMO} and ΔE_{gap} of the LNA analogue monomer nucleotides estimated at the M06-2X/6-311G(d,p) level of theory are listed in Table 4.2 and plotted in Figure 4.3, respectively. A detailed study as such on the HOMO-LUMO energies would provide an in-depth scope to relate variations in the molecular properties of the proposed antisense modifications. In case of the purine nucleobases, modifications A1, A2 have low lying E_{HOMO} and high lying E_{LUMO} and modifications A3, A4, A5 have high lying E_{HOMO} and low lying E_{LUMO} for both the nucleobases adenine and guanine. In case of the pyrimidine nucleobases, again the modifications A1, A2 have low lying E_{HOMO} and high lying E_{LUMO} and modifications A3, A4, A5 have high lying E_{HOMO} and low lying E_{LUMO} for all the three nucleobases cytosine, thymine and uracil. Now, E_{HOMO} of a molecule determines electron donating ability and E_{LUMO} determines the ability of the molecule to accept electrons. Higher the E_{HOMO} better is the electron donating capacity and lower the E_{LUMO} better is the electron accepting capacity. Thus, for both the purine and pyrimidine nucleobases there is possibility of modifications A3, A4, A5 to be better electron donors as well as better electron acceptors compared to modifications A1, A2. Accordingly, the ΔE_{gap} for modifications A3, A4, A5 were lower compared to modifications A1, A2 for both the purines and pyrimidines.

Molecular orbital compositions of the proposed LNA analogue monomer nucleotides containing nucleobases A,G,C,T,U were studied by observing the orientation and composition of their HOMO-LUMO isosurfaces, estimated at the M06-2X/6-311G(d,p) level of theory, presented in Figure 4.4. Detailed study on the molecular orbital compositions would cover an intensive scope to relate the bonding nature of the different antisense modifications bearing similar parent molecular structures. HOMO-LUMO isosurfaces of modifications A1, A2 for both A and G are majorly distributed on the nucleobase region. Being embedded within the nucleobase might decrease their

interactions with the RNase H and solvent environment. However, in the modifications A3, A4, A5 both the HOMO and LUMO isosurfaces are well distributed in the modified bridging LNA unit which will be comparatively more available for interactions with the RNase H and solvent environment.

By analysing the interactions between orbitals, Natural Bond Orbital (NBO) analysis can be particularly useful in understanding how modifications influence the properties and behavior of modified nucleic acids influence at the molecular level. NBO can provide information about stabilization energies associated with various electronic effects including charge transfer interactions and determination of bond orders between atoms which contribute to the overall stability of the molecule. This information will help in understanding the strength of bonds within, including hydrogen bonds, covalent bonds, and π-π interactions. The % contributions of each orbital to the HOMO-LUMO were calculated. Analysing the detailed orbital composition of the HOMO and LUMO, it was observed that in the modifications A1-A and A2-A, the major contributors of HOMO and LUMO are the 2p orbitals of N(18) and C(13) atoms, respectively. In modifications A3-A, A4-A, A5-A, the major contributors of both HOMO and LUMO are the 2p orbital of the C(42) atom. In modifications A1-G and A2-G, the major contributors of HOMO and LUMO are the 2p orbitals of C(15) and C(16) atoms, respectively. In modifications A3-G, A4-G, A5-G, the major contributors of both HOMO and LUMO are the 2p orbital of the C(43) atom. In the modifications A3, A4 and A5 both the HOMO and LUMO isosurfaces are well distributed in the modified bridging LNA containing region. In the modifications A1-C and A2-C, the major contributors of HOMO and LUMO are the 2p orbitals of C(3) and C(2) atoms, respectively. In modifications A3-C, A4-C, A5-C, the major contributors of both HOMO and LUMO are the 2p orbital of the C(39) atom. In modifications A1-T and A2-T, the major contributors of HOMO and LUMO are the 2p orbitals of C(10) and C(4) atoms, respectively. In modifications A3-T, A4-T, A5-T, the major contributors of both HOMO and LUMO are the 2p orbital of the C(42) atom. In modifications A1-U and A2-U, the major contributors of HOMO and LUMO are the 2p orbitals of C(10) and C(4) atoms, respectively. In modifications A3-U and A5-U, the major contributors of both HOMO and LUMO are the 2p orbital of the C(38) atom. In modification A4-U the major contributors of HOMO and LUMO are the 2p orbital of the C(39) atom and C(4) respectively. Overall, A1 and A2 have higher ΔE_{gap} for both purine and pyrimidine nucleobases and A3, A4, A5 have lower ΔE_{gap} for the same.

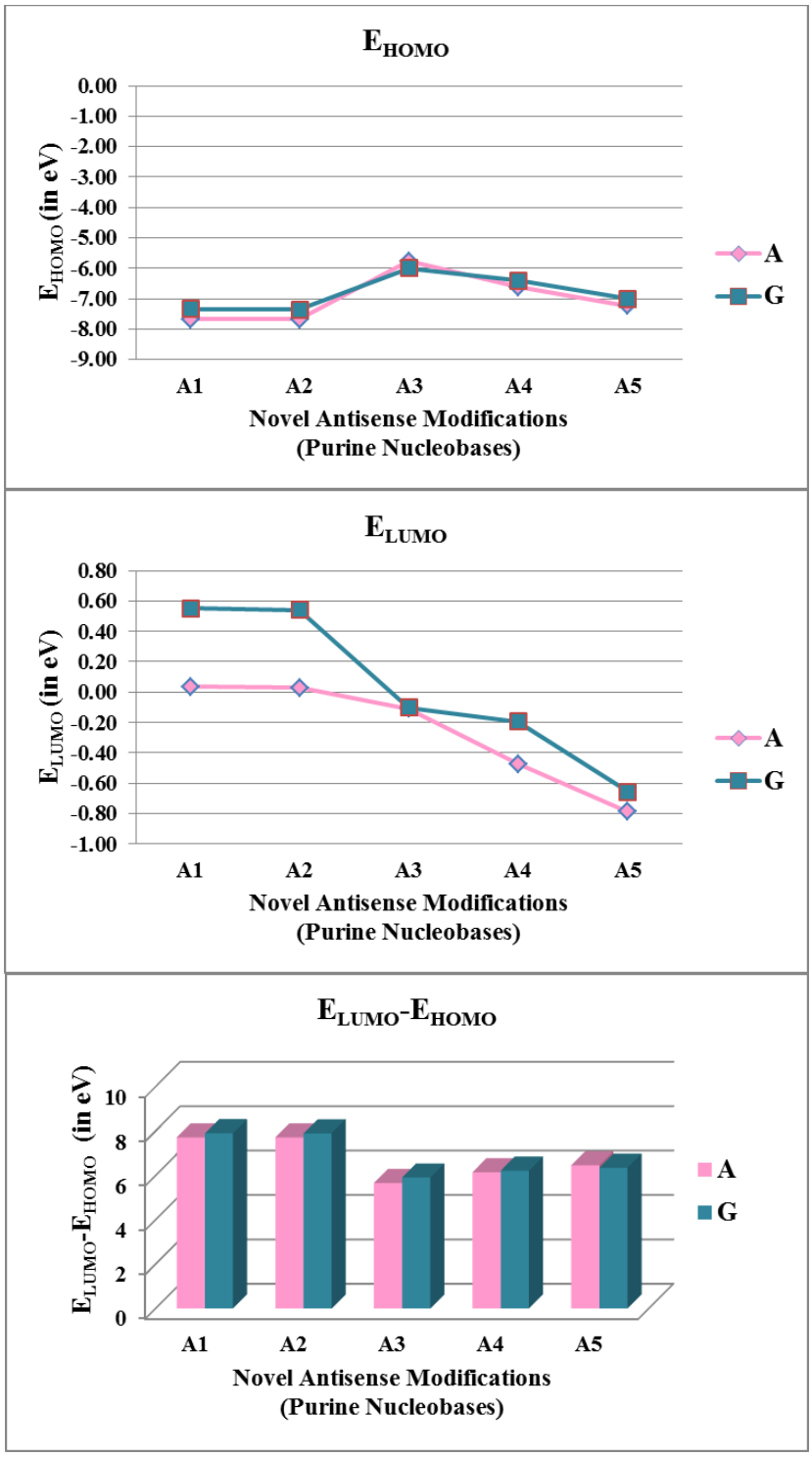
E HOMO
0.00
-1.00
-2.00
-3.00
-4.00
-5.00
-6.00
-7.00
-8.00
-9.00
E HOMO (in eV)
A1
A2
A3
A4
A5
Novel Antisense Modifications
(Purine Nucleobases)
A
G
E LUMO
0.80
0.60
0.40
0.20
0.00
-0.20
-0.40
-0.60
-0.80
-1.00
E LUMO (in eV)
A1
A2
A3
A4
A5
Novel Antisense Modifications
(Purine Nucleobases)
A
G
E LUMO-E HOMO
10
8
6
4
2
0
E LUMO-E HOMO (in eV)
A1
A2
A3
A4
A5
Novel Antisense Modifications
(Purine Nucleobases)
A
G

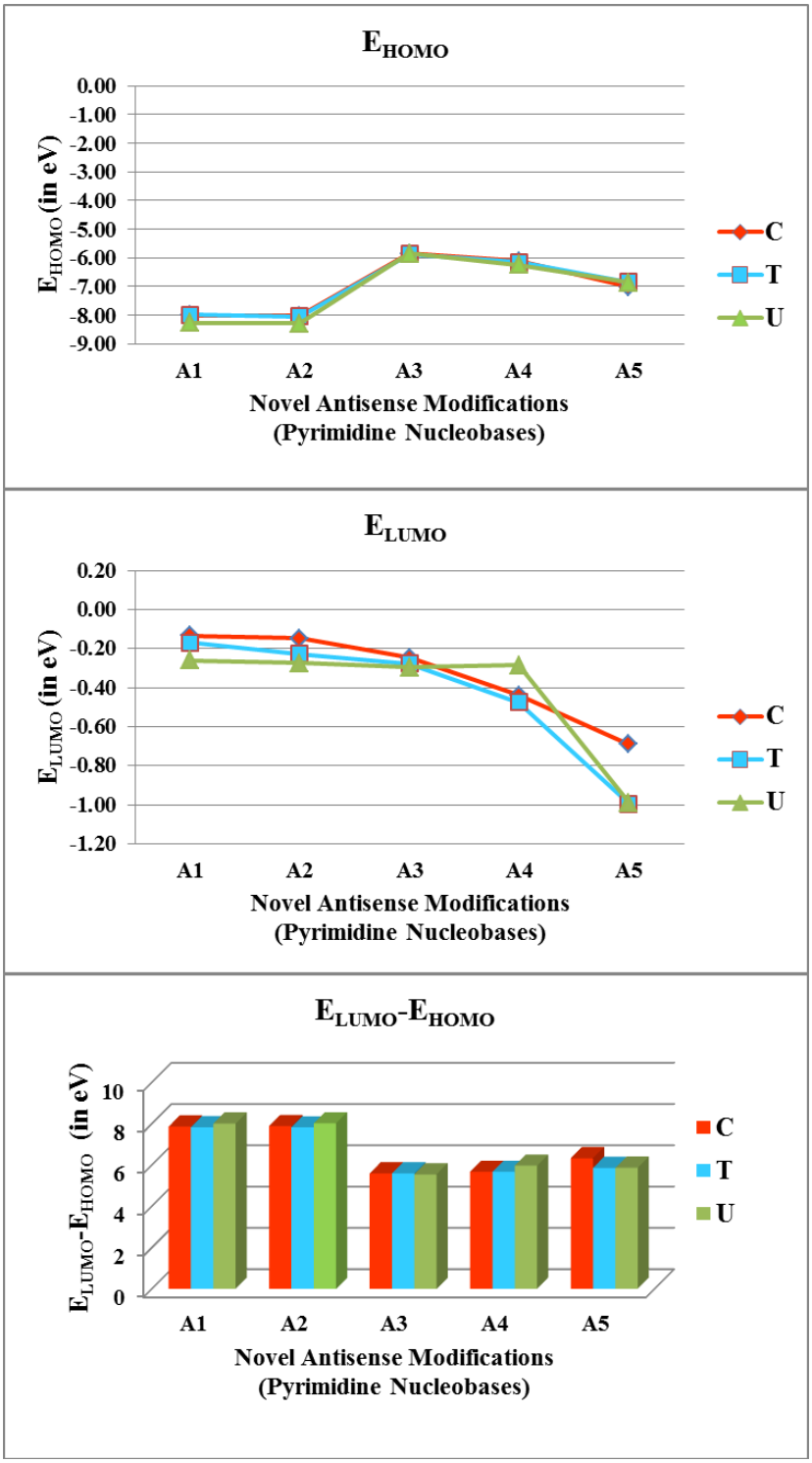

Figure 4.3: E_{HOMO}, E_{LUMO} and ΔE_{gap} of the proposed LNA analogue antisense modifications A1, A2, A3, A4, A5 with their respective nucleobases Adenine(A), Guanine(G), Cytosine(C), Thymine(T) and Uracil(U) calculated at the M06-2X/6-311G(d,p) level of theory.

(a) Nucleobase: Adenine (A)

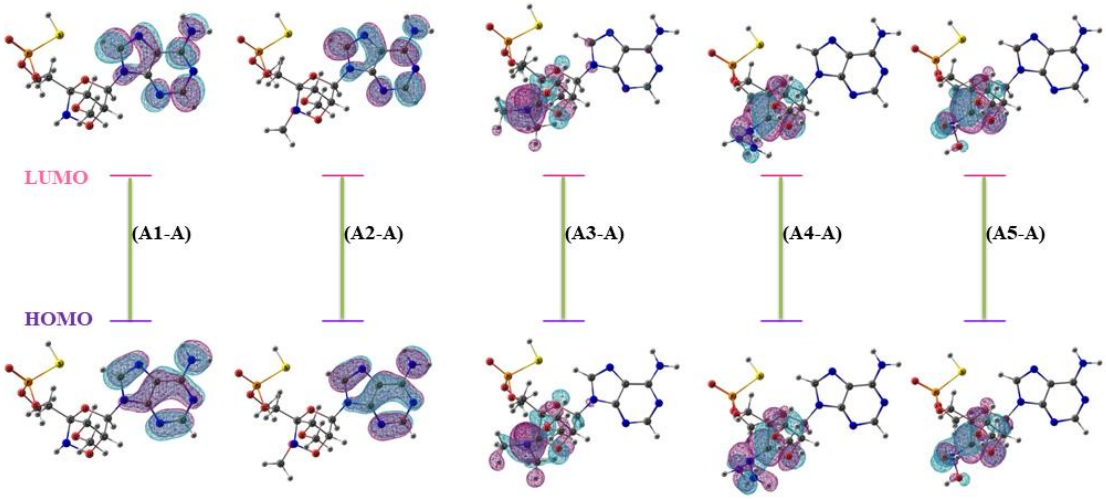

(b) Nucleobase: Guanine (G)

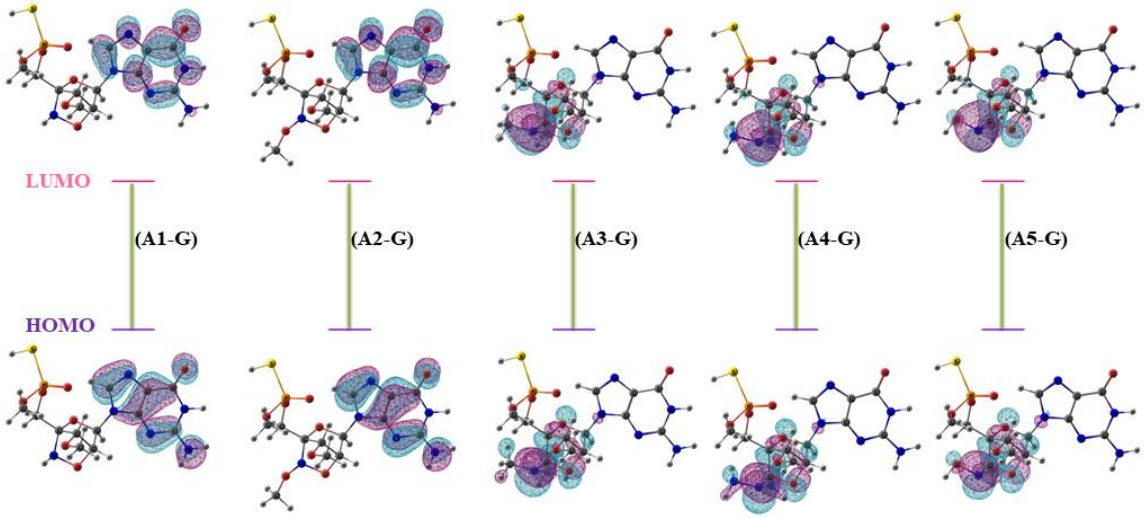

(c) Nucleobase: Cytosine (C)

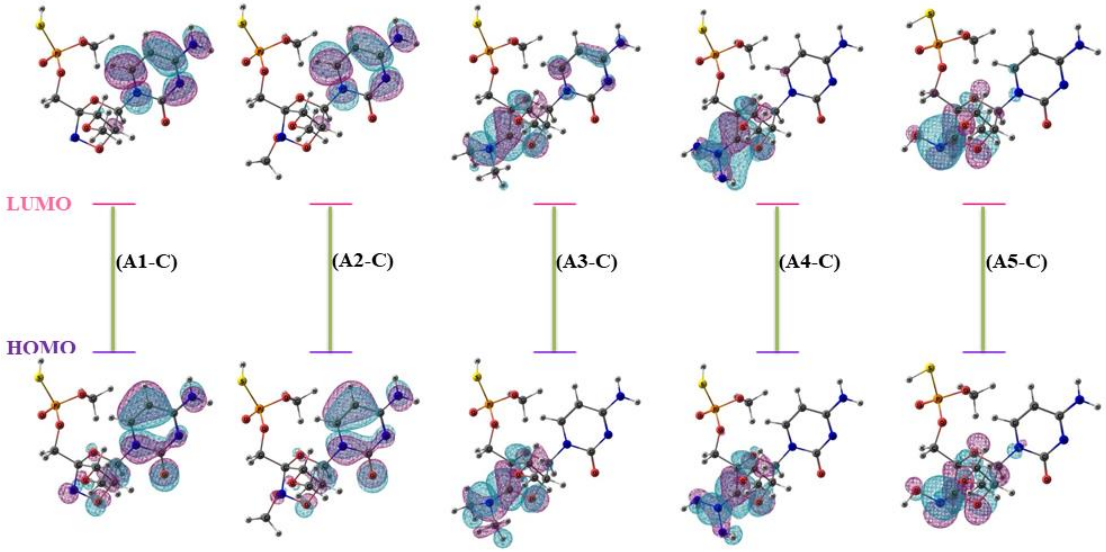

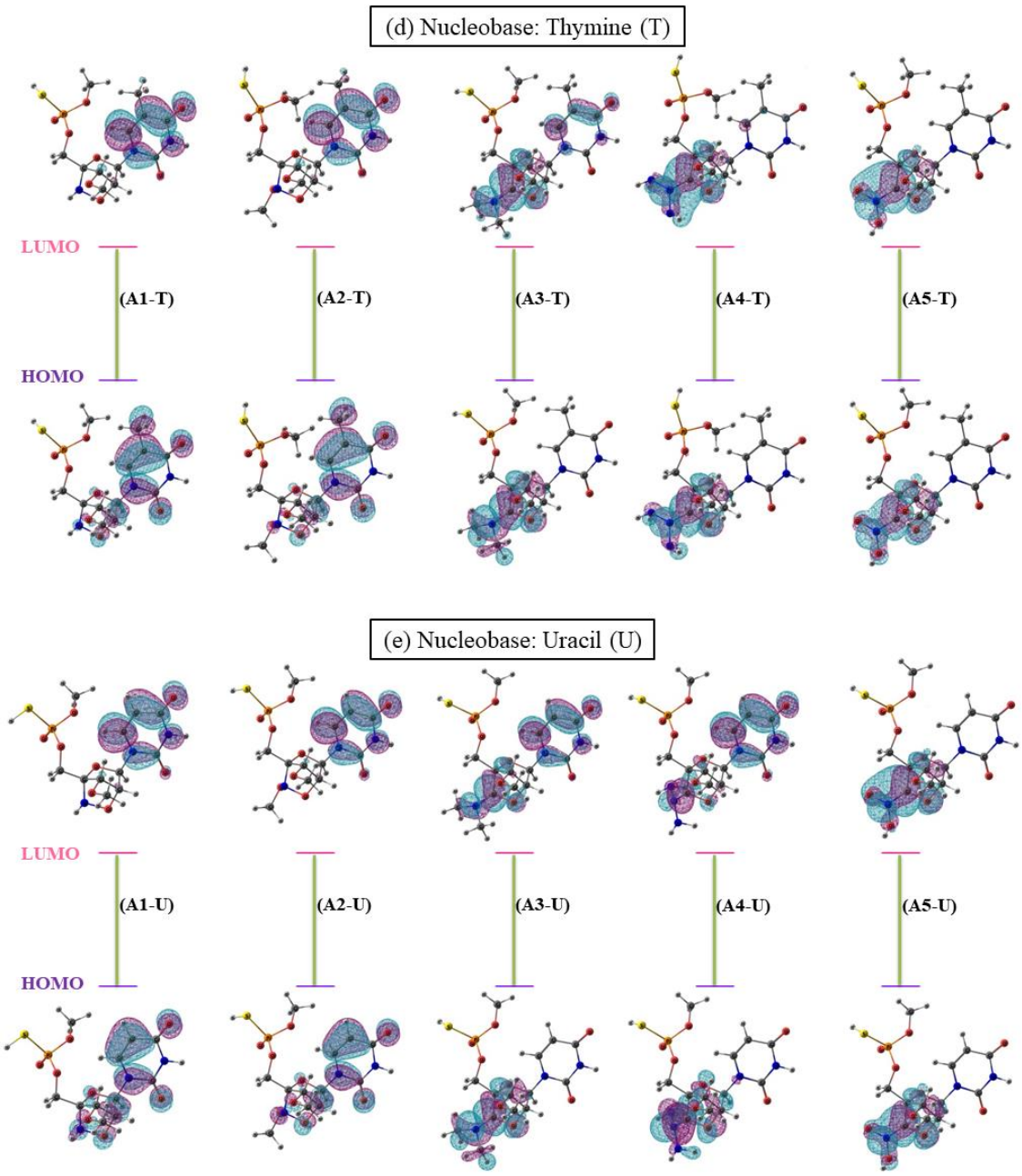

Figure 4.4: HOMO, LUMO iso-surfaces of monomer nucleotides of the proposed LNA analogue antisense modifications (A1-A5) each containing nucleobase (a) Adenine(A), (b) Guanine(G), (c) Cytosine(C), (d) Thymine (T) and (e) Uracil (U) respectively calculated at the M06-2X/6-311G(d,p) level of theory.

4.3.1.3. Global reactivity descriptors of the LNA analogue monomer nucleotides

A brief analysis on the HOMO-LUMO energies is of ample importance considering the bonding nature of molecules. But, alongside that, a detailed study on the global reactivity descriptors derived from the HOMO-LUMO energies can provide an in-

depth scope to predict the drug like nature of the proposed antisense alterations. According to these descriptors, extent of chemical reactivity and stability of a molecule varies with changing structural configuration of the molecules. Such type of study has been used by several research groups for small drug molecules and their derivatives bearing similar molecular structures including a few modified nucleobases as well. In the present work, we have used a similar strategy to study the quantum chemical reactivity descriptors of monomer nucleotides of the proposed LNA analogue antisense modifications. Calculated global reactivity descriptors global hardness (η), global softness (S), chemical potential (μ) and electrophilicity (ω) of the monomer nucleotides of the proposed LNA analogue antisense modifications (A1-A5) with their respective nucleobases A,G,C,T,U estimated at the M06-2X/6-311G(d,p) level of theory are shown Figure 4.5 and listed in Table 4.3, respectively.

Global hardness (η) and global softness (S) gives us a qualitative demonstration of how polarizable a molecule is and gives us an indication of resistance to deformation. Hard molecules do not have easily excitable outer electrons and are less polarizable. It is associated with low lying E_{HOMO} and high lying E_{LUMO}. Qualitatively global softness (S) is the reciprocal of hardness. Associated with high lying E_{HOMO} and low lying E_{LUMO} soft molecules have easily accessible outer electrons and are more polarizable compared to the hard molecules. Thus, hard molecules will have a higher ΔE_{gap} compared to soft molecules. In general, a molecule with high a ΔE_{gap} is considered chemically more stable while a small ΔE_{Gap} is considered chemically more reactive. Results from ΔE_{Gap}, global hardness (η) and global softness (S) revealed that modifications A3, A4, A5 will be more active in electron receiving and elimination processes or softer in chemical reactions compared to modifications A1, A2 irrespective of the type of nucleobase be it the purines or the pyrimidines. Chemical potential (μ) and electrophilicity (ω) are two further associated metrics that can be utilized to estimate the monomer nucleotides relative reactivity. The chemical potential (μ) mentioned here is the electronic chemical potential that measures an infinitesimal change in energy upon addition of an electronic charge. Results from chemical potential (μ) values suggests that modifications A1, A2, A5 have more negative chemical potential values and modifications A3, A4 have less negative chemical potential values for the purines and on the other hand modifications A1, A2, have more negative chemical potential values and modifications A3, A4, A5 have less negative chemical potential values for the pyrimidines.

Table 4.3: Global hardness (η), Global softness (S), Chemical potential (μ) and Electrophilicity (ω) of the proposed LNA analogue antisense modifications A1, A2, A3, A4, A5 with their respective nucleobases Adenine(A), Guanine(G), Cytosine(C), Thymine(T) and Uracil(U) calculated at the M06-2X/6-311G(d,p) level of theory.

Nucleobases	Name Code	Global Hardness (η)	Global Softness (S)	Chemical Potential (μ)	Electrophilicity (ω)
Adenine	A1-A	3.86	0.130	-3.819	1.892
	A2-A	3.86	0.130	-3.827	1.899
	A3-A	2.83	0.177	-2.937	1.525
	A4-A	3.07	0.163	-3.546	2.047
	A5-A	3.23	0.155	-4.014	2.497
Guanine	A1-G	3.95	0.127	-3.395	1.459
	A2-G	3.95	0.127	-3.406	1.470
	A3-G	2.95	0.169	-3.054	1.580
	A4-G	3.10	0.161	-3.298	1.752
	A5-G	3.17	0.158	-3.828	2.310
Cytosine	A1-C	3.93	0.127	-4.067	2.103
	A2-C	3.94	0.127	-4.090	2.121
	A3-C	2.80	0.179	-3.045	1.656
	A4-C	2.83	0.176	-3.273	1.890
	A5-C	3.16	0.158	-3.854	2.347
Thymine	A1-T	3.91	0.128	-4.082	2.128
	A2-T	3.91	0.128	-4.137	2.188
	A3-T	2.80	0.179	-3.078	1.691
	A4-T	2.83	0.176	-3.309	1.931
	A5-T	2.93	0.171	-3.921	2.626
Uracil	A1-U	4.00	0.125	-4.263	2.269
	A2-U	4.01	0.125	-4.282	2.288
	A3-U	2.77	0.180	-3.071	1.700
	A4-U	2.98	0.168	-3.268	1.789
	A5-U	2.94	0.170	-3.924	2.622

An indicator of a system's responsiveness to nucleophiles and electrophiles, electrophilicity (ω) is connected to the stabilization of energy when a system becomes saturated with electrons from the outside environment. Lower values of ω indicate presence of a good nucleophilic character, while higher values of ω indicate the presence

of a good electrophilic character. Electrophilicity values suggest that modifications A3, A4 are less electrophilic while modifications A1, A2, A5 are more electrophilic irrespective of the type of nucleobase be it the purines or the pyrimidines. This is an implication of A3, A4 having high lying E_{HOMO} which will accept electrons less easily, rather will donate more easily and hence less electrophilic, compared to A1, A2, A5 having low lying E_{HOMO} which will donate electrons less easily, rather will accept more easily and hence more electrophilic. Overall, modifications A3, A4 have less negative chemical potential and are less electrophilic compared to A1, A2, A5 for both the purine and pyrimidine nucleobases.

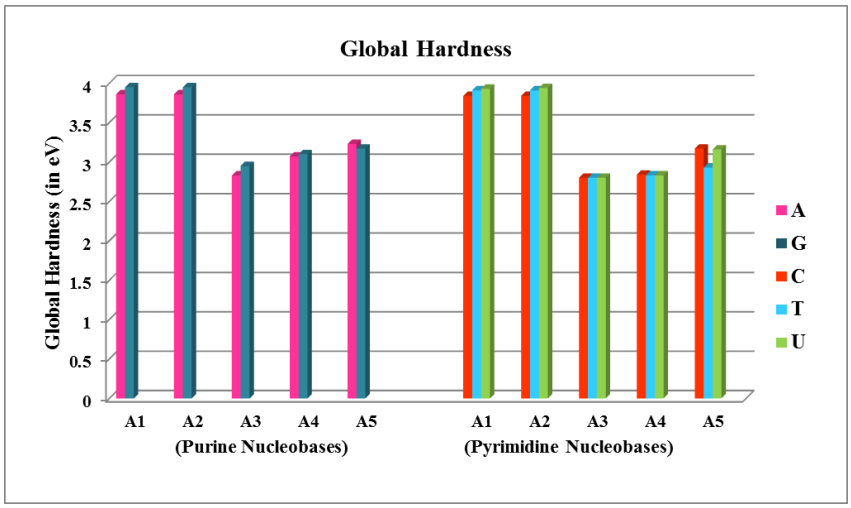

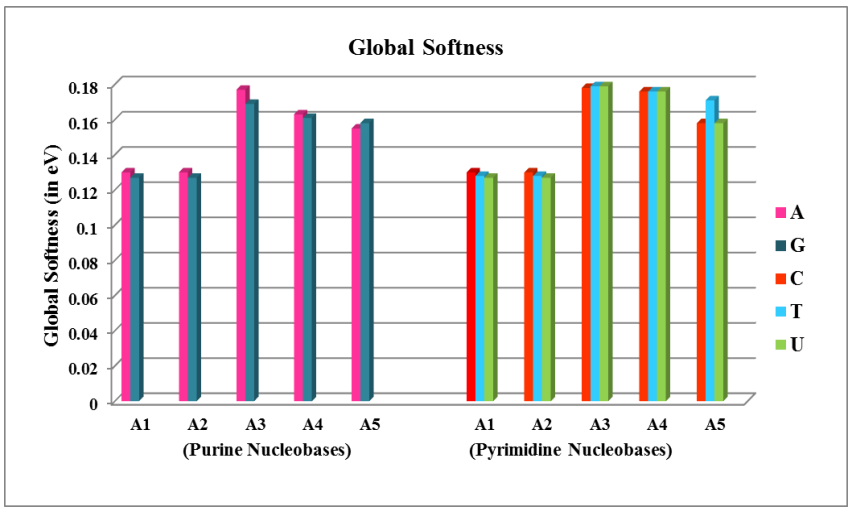

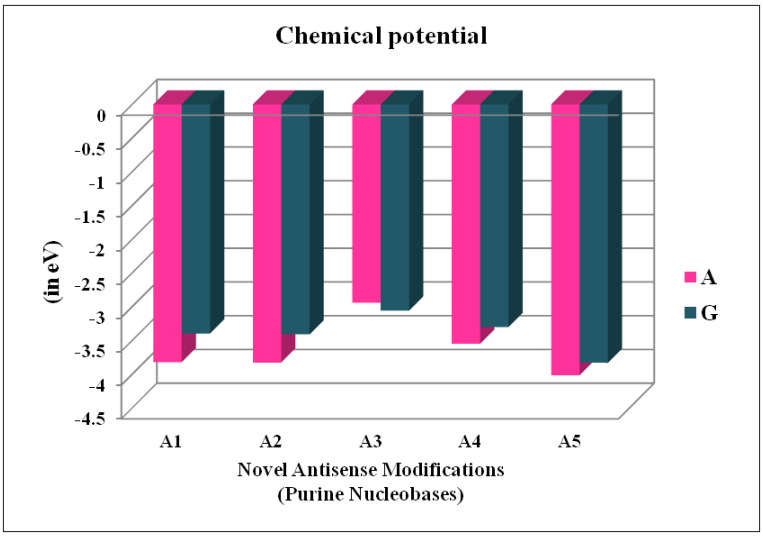
Chemical potential
0
-0.5
-1
-1.5
-2
-2.5
-3
-3.5
-4
-4.5
(in eV)
A1
A2
A3
A4
A5
Novel Antisense Modifications
(Purine Nucleobases)
A
G

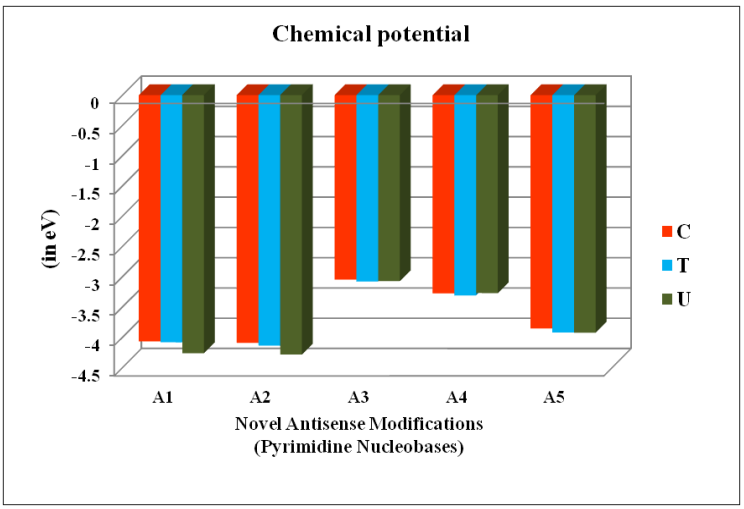
Chemical potential
0
-0.5
-1
-1.5
-2
-2.5
-3
-3.5
-4
-4.5
(in eV)
A1
A2
A3
A4
A5
Novel Antisense Modifications
(Pyrimidine Nucleobases)
C
T
U

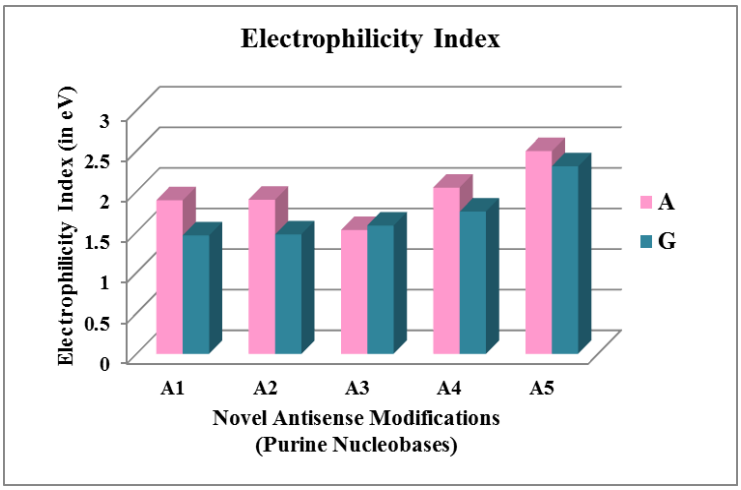
Electrophilicity Index
Electrophilicity Index (in eV)
3
2.5
2
1.5
1
0.5
0
A1
A2
A3
A4
A5
Novel Antisense Modifications
(Purine Nucleobases)
A
G

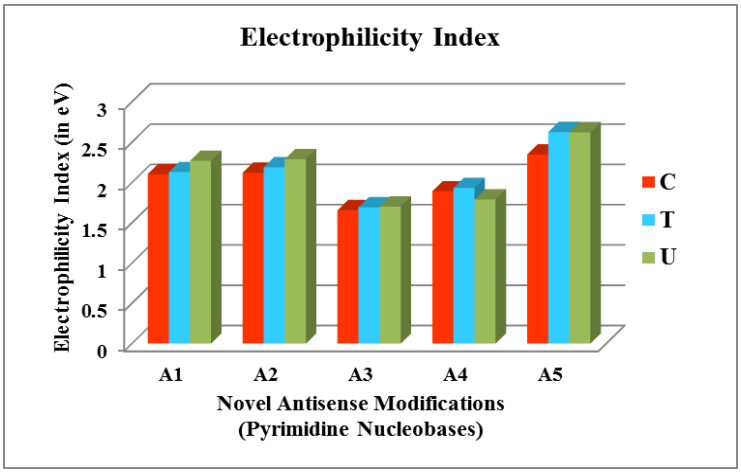

Figure 4.5: Global hardness (η), Global softness (S) Chemical potential (μ) and Electrophilicity (ω) of the proposed LNA analogue antisense modifications A1, A2, A3, A4, A5 with their respective nucleobases Adenine(A), Guanine(G), Cytosine(C), Thymine(T) and Uracil(U) calculated at the M06-2X/6-311G(d,p) level of theory.

4.3.2. MD Simulation Results

4.3.2.1. Dynamics of the proposed LNA analogue ASO/RNA oligomer duplexes

Experimenting design possibilities of novel LNA analogues has resulted into numerous LNA antisense alterations of being investigated for a variety of potential biological activities. Being incorporated into the oligomeric nucleic acid duplexes, the proposed modifications will reorganize the structural and dynamic properties of the modified ASO/RNA duplexes as a whole. Also, it is unwise to design the analogues without first confirming their ability to strongly duplex with the targets, particularly a natural source as mRNA. Thus, detailed MD simulation study was carried on fully modified 14-mer (5′-CTTAGCACTGGCCT-3′/3′-GAAUCGUGACCGGA-5′) ASO/RNA hybrids containing the modifications (A1-A5), over 100 ns simulation trajectory data. 100 ns sampling time of the simulation was considered noting the smaller size of the duplexes. Previous experimental studies targeting protein PTEN using LNA and MOE modifications in mouse have resulted in an increased potency of second generation ASOs by reducing the length of the ASOs from 20-mer to 14-mer [37-39]. They have been reported to demonstrate excellent safety profile in human clinical trials as well. Additionally, although it has been reported of higher antisense activity of chimeric ASO-(PS-DNA)-ASO/RNA gapmer duplexes, however fully modified ASO/RNA duplexes have been considered in the present work to study the influence and

differentiate the properties of the proposed modifications over parent LNA ASOs and to particularly compare the same with already reported fully modified LNA/RNA duplexes.

Structures of the 14-mer ASO/RNA duplexes (a) LNA/RNA (b) A1/RNA (c) A2/RNA (d) A3/RNA (e) A4/RNA and (f) A5/RNA considered for the simulation study are shown in Figure 4.6. Since the modifications are LNA based, a fully modified LNA/RNA hybrid has been considered as the control system for comparison. All the six duplexes were observed to be right-handed trying to adopt typical *A-form* duplex configurations. The modified 2′C-4′C bridges were located towards the edge of the minor groove with no steric hindrance for duplex formation. The *N*-glycosidic dihedral angles were in *anti*-conformation maintaining stable *Watson-Crick* base-pairing for all the base pairs throughout the duplex. Identical base-stacking pattern was also observed for all the ASO/RNA duplexes similar to the LNA/RNA control system. Thus, the base-pairing and base-stacking patterns were not altered by incorporation of the proposed antisense modifications. The overall appearance of the duplexes was right-handed helical with apparent *Watson-Crick* base-pairing, base-stacking pattern and all participating nucleotides in *anti*-conformations well described in the subsequent sections.

Structures obtained from the entire simulation trajectory were then compared with their respective initial structures by analyzing their RMSD plots presented covering the entire duplex, plotted in Figure 4.7 and RoG plots in Figure 4.8. Information of RMSD versus time for the ASO/RNA duplexes showed that duplex stability is well maintained for the entire simulation time in each case. Visual inspection of the trajectories showed that each of the duplexes was fluctuating potentially in and around a range of 2Å to 5Å of RMSD values. Earlier simulation studies on 14-mer gapmer duplexes with LNA and MOE modifications depicted RMSDs of ~2-6 Å for complete duplexes and ~1-3 Å for the non-terminal base pairs [45]. Calculated average RMSD values of LNA contained duplex exhibited an average RMSD of 4.87Å and duplexes containing modifications A1, A2, A3, A4, A5 exhibited average RMSDs of 4.64, 4.52, 5.60, 4.89, 5.36 Å respectively. A1/RNA, A2/RNA duplexes exhibited relatively lower and A3/RNA, A4/RNA, A5/RNA duplexes exhibited relatively higher RMSDs compared to the LNA/RNA control system. From the overall results, the modified ASO/RNA duplexes in the present study exhibited stable RMSD's compared to the reported LNA and MOE contained ASO/RNA hybrids.

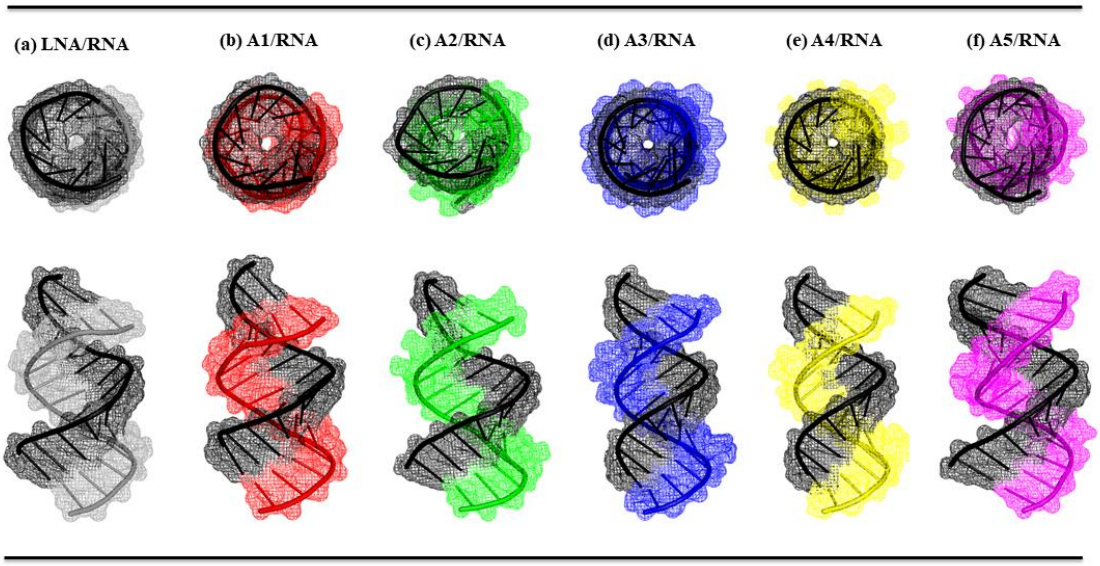

Figure 4.6: Structures of 14-mer ASO/RNA duplexes (a) LNA/RNA (b) A1/RNA (c) A2/RNA (d) A3/RNA (e) A4/RNA and (f) A5/RNA considered for the MD simulation study.

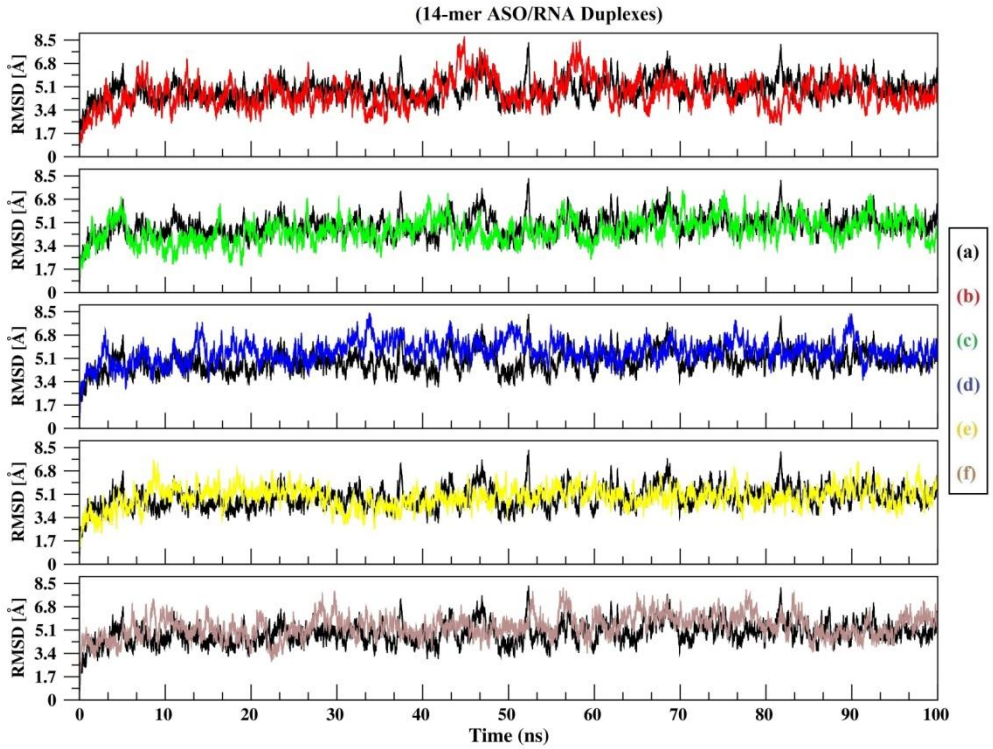

Figure 4.7: RMSD plots of the 14-mer ASO/RNA duplexes (a) LNA/RNA (b) A1/RNA (c) A2/RNA (d) A3/RNA (e) A4/RNA and (f) A5/RNA for the entire simulation trajectory.

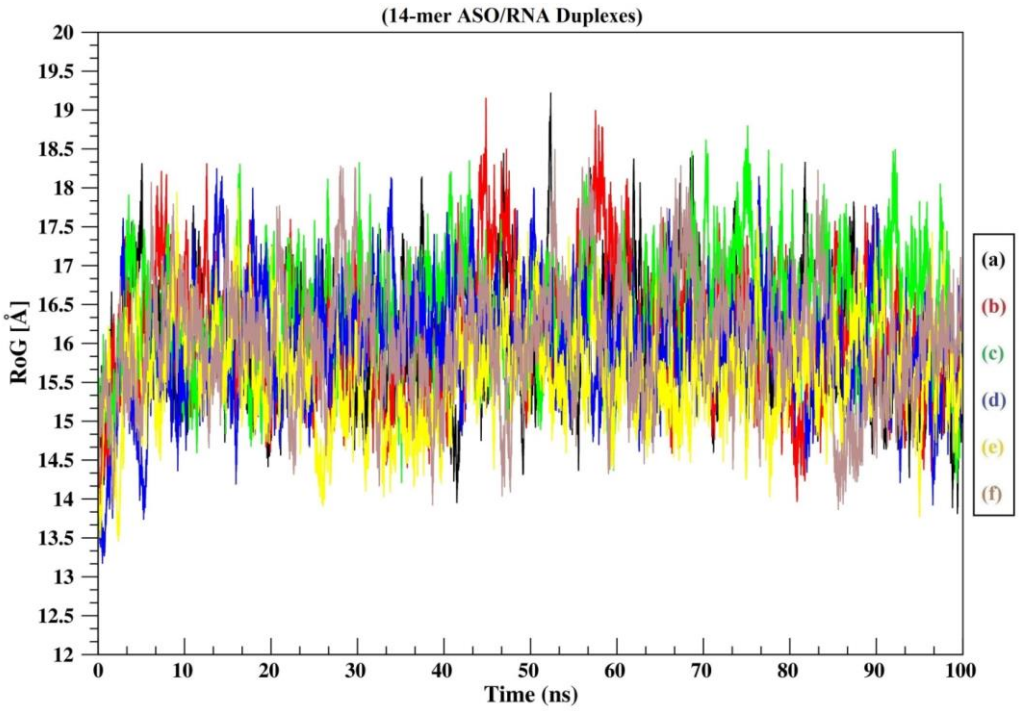

Figure 4.8: RoG plot of the 14-mer ASO/RNA duplexes (a) LNA/RNA (b) A1/RNA (c) A2/RNA (d) A3/RNA (e) A4/RNA and (f) A5/RNA for the entire simulation trajectory.

4.3.2.2. Oligomer Duplex Dynamic Structure: Inter-Strand and Intra-Strand PP distances

The structural framework of nucleic acid duplexes comprises of two sugar-phosphate backbones twisted together to form the molecular double helix. The *C2'-endo* sugar puckering seen in *B-type* duplexes is described by longer intra-strand phosphate-phosphate (PP) distances (~7Å) while the *C3'-endo* sugar puckering seen in *A-type* duplexes is described by lower intra-PP distances (~5.9Å) [75-76]. Average inter-PP and intra-PP distances of the modified ASO/RNA duplexes for both the strands for the entire simulation trajectory are plotted in Figure 4.9.

Monomer nucleotides from the LNA/RNA duplex were exhibiting intra-PP distance <6.2 Å for the RNA strand residues and ~6.8 Å for the LNA strand residues. For the ASO/RNA duplexes, the RNA strands residues were exhibiting highly flexible intra-PP distances ranging from ~5.8-6.9 Å and in a similar way, nucleotide residues from the ASO strands were also exhibiting variable intra-PP distances ranging from ~5.1-6.8 Å. Understanding these inter-strand and intra-strand PP distances in modified DNAs is crucial for elucidating their structural properties, stability, and functional roles in biological processes.

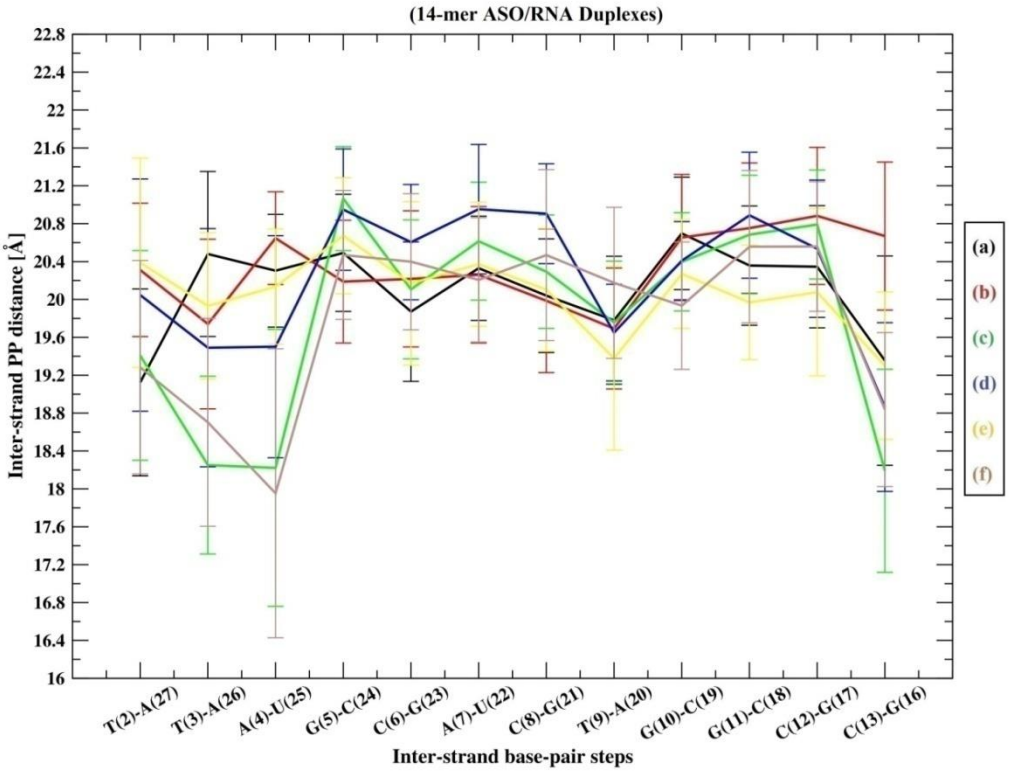
(14-mer ASO/RNA Duplexes)
Inter-strand PP distance [Å]
22.8
22.4
22
21.6
21.2
20.8
20.4
20
19.6
19.2
18.8
18.4
18
17.6
17.2
16.8
16.4
16
T(2)-A(27)
T(3)-A(26)
A(4)-U(25)
G(5)-C(24)
C(6)-G(23)
A(7)-U(22)
C(8)-G(21)
T(9)-A(20)
G(10)-C(19)
G(11)-C(18)
C(12)-G(17)
C(13)-G(16)
Inter-strand base-pair steps
(a)
(b)
(c)
(d)
(e)
(f)

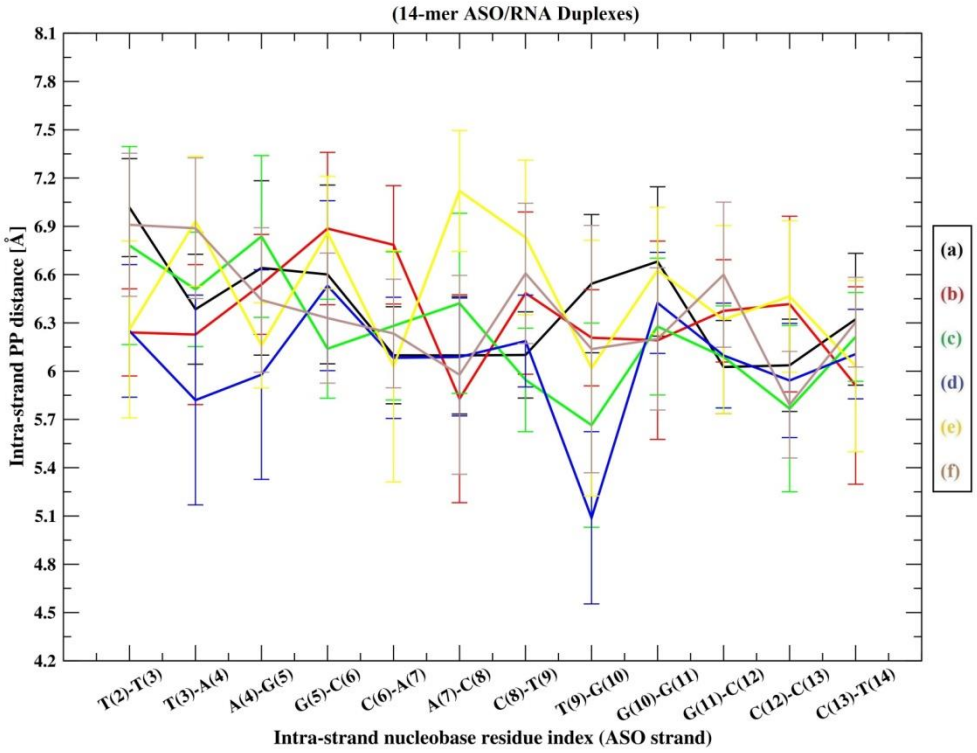
(14-mer ASO/RNA Duplexes)
Intra-strand PP distance [Å]
8.1
7.8
7.5
7.2
6.9
6.6
6.3
6
5.7
5.4
5.1
4.8
4.5
4.2
T(2)-T(3)
T(3)-A(4)
A(4)-G(5)
G(5)-C(6)
C(6)-A(7)
A(7)-C(8)
C(8)-T(9)
T(9)-G(10)
G(10)-G(11)
G(11)-C(12)
C(12)-C(13)
C(13)-T(14)
Intra-strand nucleobase residue index (ASO strand)
(a)
(b)
(c)
(d)
(e)
(f)

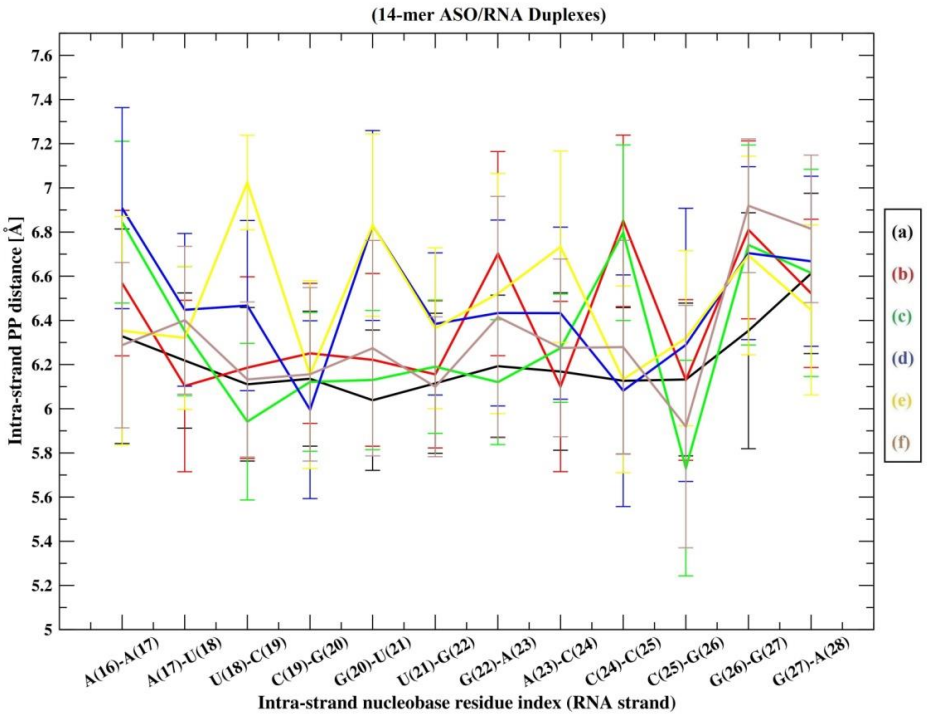

Figure 4.9: Inter-strand and Intra-strand PP distances of the 14-mer ASO/RNA duplexes (a) LNA/RNA (b) A1/RNA (c) A2/RNA (d) A3/RNA (e) A4/RNA and (f) A5/RNA for both the strands for the entire simulation trajectory.

4.3.2.3. Torsion Angle Dynamics: Sugar-pucker and N-glycosidic torsion angle distribution

Base-pairing, base-stacking are directly correlated with the sugar puckering distribution of the nucleotides and accordingly upon the orientation of the phosphate backbone relative to the sugar or the nucleobases. Differences in non-bonded conflicts caused by the *C2′-endo* versus *C3′-endo* conformations are clearly reflected in the correlations between the nucleotides sugar-puckering and *N-glycosidic* dihedral angles. Nucleic acids contain sugar puckers that are either in the *C3′-endo* (pucker phase values: 0°–40°) or the *C2′-endo* (pucker phase values: 120°–180°) conformation which correspond to the *A-form* or *B-form* conformations in a duplex, respectively. According to earlier NMR structures and MD simulation studies on LNA ASOs, LNA steers a larger population of the sugar puckers into the *C3′-endo* conformation in an effort to create an overall *A-form* geometry. To predict the magnitude of such conformational integration of the modified LNA ASOs sugar pucker distribution of the nucleotide residues throughout the duplex for the modified ASO/RNA duplexes are plotted in Figure 4.10. As seen in Figure 4.10, sugar puckers of all the nucleotides from the ASO strand lie in the range of 0°-40° inferring that the nucleotides were in C3′-*endo* conformation throughout the

simulation period. As for the RNA strands, residues although majority of the residues were exhibiting *C3′-endo* conformation however a few were seen to fluctuate from ideal *C3′-endo* conformation exhibiting a in between *C3′-endo* and the *C2′-endo* conformations. Thus, residues from the ASO strands containing the proposed LNA analogue antisense modifications are clearly visible influencing the sugar puckering pattern on their complementary RNA strands.

N-glycosidic dihedral angle measures the influence of the modifications on the distance between the atoms bonded directly to the C1′ carbon that forms the glycosidic bond with RNA. The *N-glycosidic* bond and the corresponding chi (χ) torsion angle illustrate that the nucleobase and sugar are two separate entities and that there is an internal degree of freedom between them. The *N-glycosidic* dihedral angle chi (χ) was calculated to explore the rigidity and dependency of each modified nucleotide on the sugar-nucleobase orientation such that the modified nucleotides exist in an anti-conformation, a property of *A-form* helix observed in RNAs. Although chi (χ) is capable of adopting a large range of values, structural restrictions limit the values for well-defined preferences. It has been already discussed that the chi (χ) torsion angle defined by the O4′-C1′-N9-C4 atoms for purines and O4′-C1′-N1-C2 atoms for pyrimidines specifies the relative sugar-nucleobase orientation in standard nucleic acids. Two main low-energy conformations for the *A-form* and *B-form* duplexes were predicted by theory in accordance with experimental results, where ranges of +90° to +180°; -90° to -180° (or 180° to 270°) corresponds to the *anti*-conformation and values in the range of -90° to +90° corresponds to the *syn*-conformation. The *syn* glycosidic angles are uncommon in nucleotides with C3′-endo sugar puckers due to the steric conflict between the nucleobase and the H3′ atom, which is pointed towards the base in this specific pucker mode. *N-glycosidic* torsion distribution of the monomer nucleotides from both the strands of the ASO/RNA duplexes are plotted in Figure 4.11. Monomer nucleotides from the modified ASO/RNA duplexes were exhibiting chi (χ) values strictly ranging between -120° to -180° for the ASO strand residues and values ranging from -60° to -180° for the RNA strand residues. Although residues from the ASO strands containing the proposed LNA analogue antisense modifications were seen influencing the *N-glycosidic* torsion distribution on their complementary RNA strands yet the duplexes were trying to maintain their relative sugar-base orientations to be in *anti*-conformation maintaining stable *Watson-Crick* base pairing throughout the duplex for the entire simulation time.

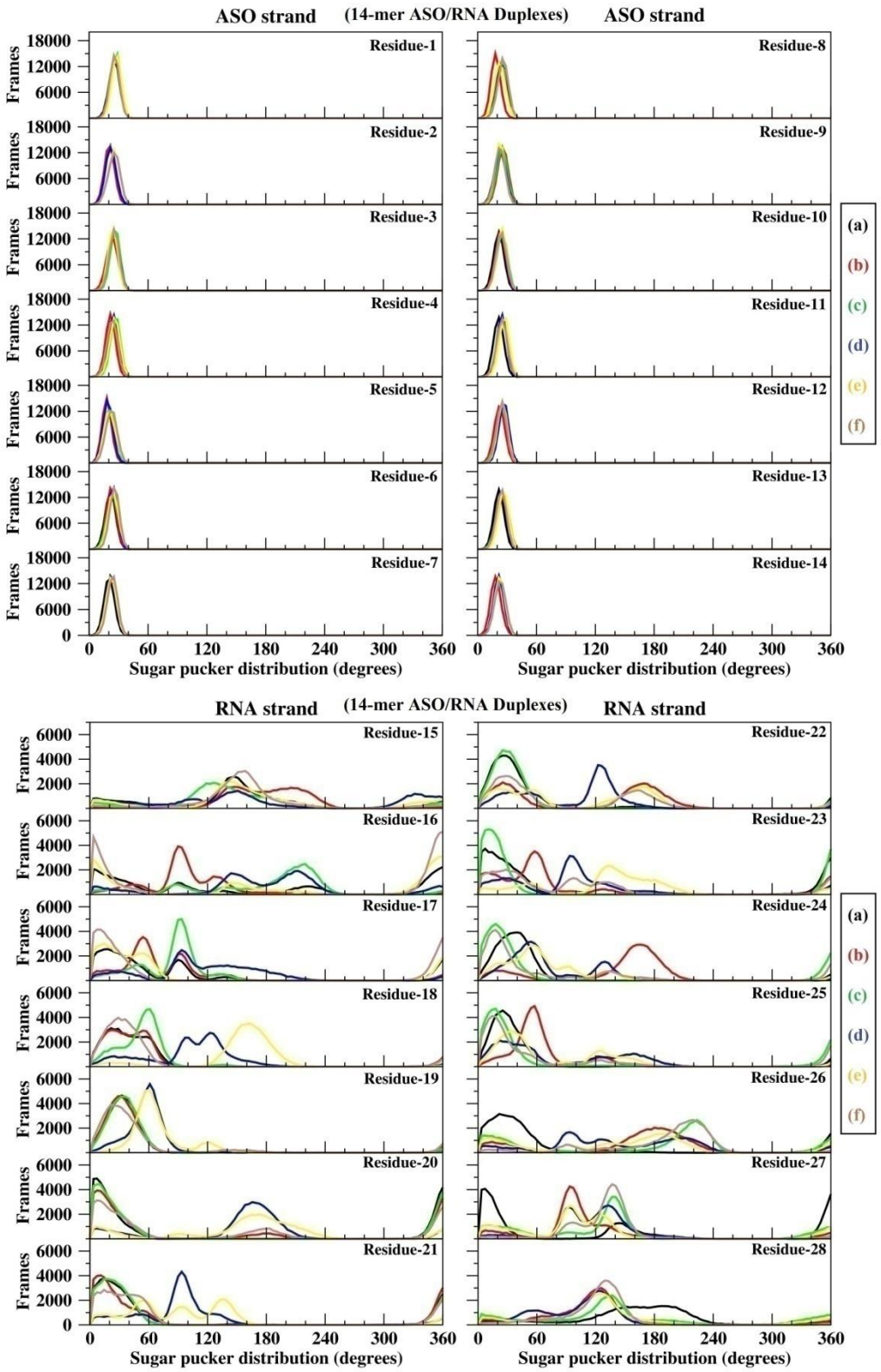

Figure 4.10: Sugar puckering of the 14-mer ASO/RNA duplexes (a) LNA/RNA (b) A1/RNA (c) A2/RNA (d) A3/RNA (e) A4/RNA and (f) A5/RNA for the entire simulation trajectory.

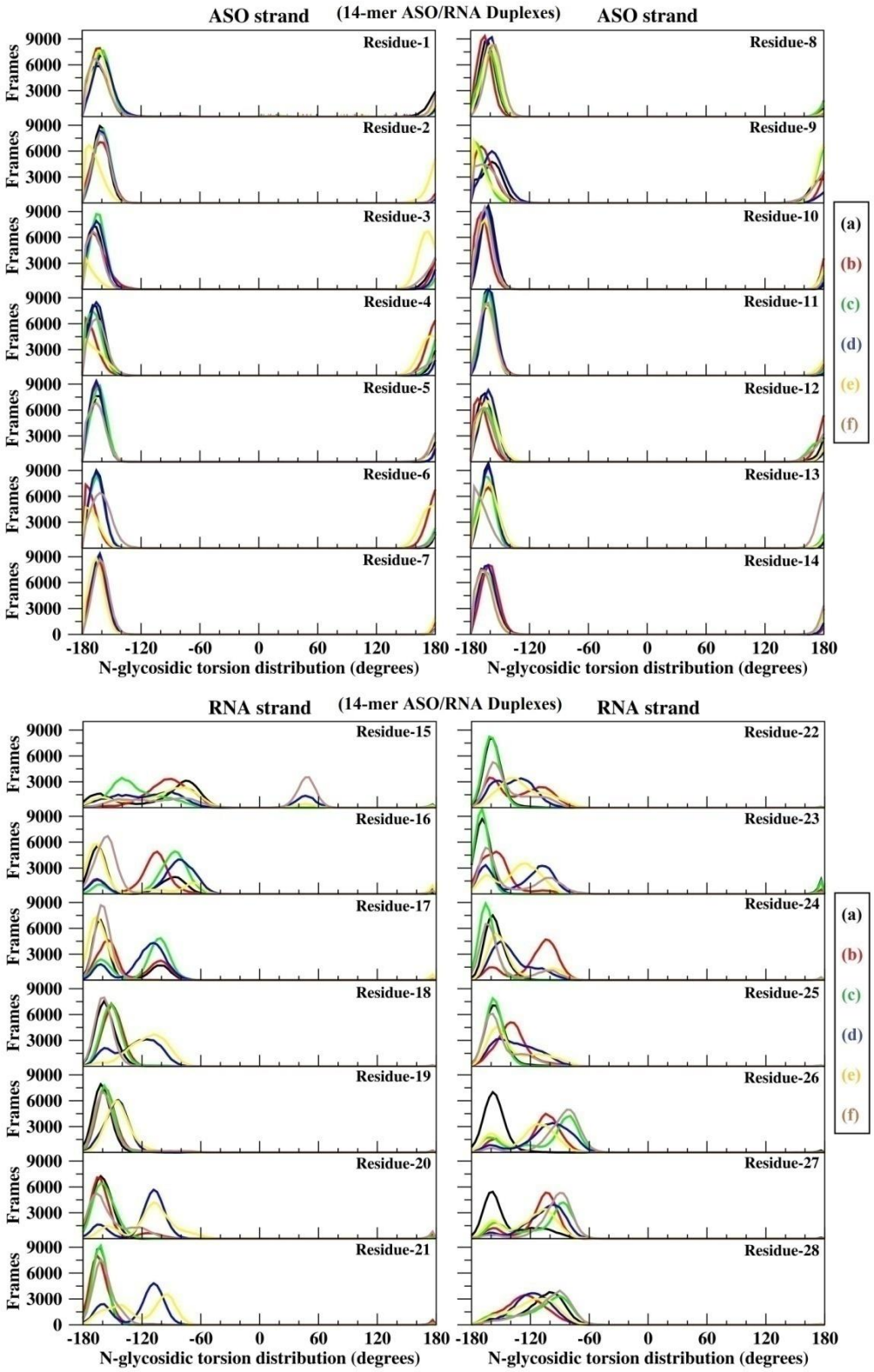

Figure 4.11: N-glycosidic dihedral of the 14-mer ASO/RNA duplexes (a) LNA/RNA (b) A1/RNA (c) A2/RNA (d) A3/RNA (e) A4/RNA and (f) A5/RNA for the entire simulation trajectory.

4.3.2.4. Backbone flexibility, Base-pairing, Base-stacking and H-Bond interactions

The **s**ugar-phosphate backbone of nucleic acid duplexes provides directionality and flexibility to the nucleotides throughout the duplex. Modifications to this backbone, such as changes in the sugar moiety or the phosphodiester linkage, can alter the flexibility of the duplex. Understanding the flexibility of the **s**ugar-phosphate backbone is crucial for predicting how modified nucleic acids interact with proteins, enzymes, and other nucleic acids. Now, flexibility of the **s**ugar-phosphate backbone is reported to play a major role in Human RNase H recognition of antisense duplexes. The active site of the enzyme comprises of an RNA-binding groove and a spatially conserved phosphate-binding pocket which defines a DNA-binding site. Specific binding of the DNA/RNA duplexes is highly dependent on the surface complementarity and close fitting of the sugar-phosphate backbone of the DNA, making *van der Waals* contacts and H-bond interactions at the active site of RNase H. Depending on the flexibility of the backbone, the minor groove width of the DNA/RNA duplexes changes at the phosphate binding pocket of the DNA-binding channel. Backbone flexibility thus plays a significant role on imparting dominant antisense activity when it comes to modified ASO/RNA duplexes. Fully modified LNA duplexes are reported to exhibit low backbone flexibility and to not force their flexibility on their complementary partner strands. To explore the influence of the proposed modifications on duplex backbone flexibility residue wise RMSF of backbone heavy atoms were calculated for each nucleotide from both the nucleic acid strands plotted in Figure 4.12. In general, nucleic acid duplexes, the terminal residues show high fluctuations compared to the non-terminal residues. Accordingly, terminal residues of the ASO/RNA duplexes demonstrated high fluctuations compared to the non-terminal residues. Comparing the non-terminal residues of all the duplexes, the A1, A2, A5 modified ASO strands influenced their complementary RNA strands such that both the strands exhibited low backbone flexibility compared to the LNA/RNA duplex. However, A3/RNA and A4/RNA exhibited higher flexibility compared to the LNA/RNA control system for both the sense and antisense strand, thus suggesting these modifications to be highly flexible compared to the parent LNA modification thus serving the very purpose of its creation.

Base pairing is immensely essential for functional RNAs as the folded structure of the RNA molecules are highly stabilized by their base pairing interactions which utilize the 2′-OH group of the ribose sugar ring [77-78]. The proposed modifications

being 2′-OH modified would thus affect the active base pairing conformations of the modified ASO/RNA duplexes. To bind sequence specifically to their target RNAs the modified monomer nucleotides should form effective base pairing with the RNA nucleotides, for which, the same should exist in an *anti*-conformation, a property of *A-form* helix generally observed in RNAs [79]. Also, the modified nucleotides in complex with the RNAs should induce the RNA nucleotides to adopt or retain an *N-type* conformation favouring *C3'-endo* sugar puckering which will reduce conformational flexibility of the ribose sugar and increase local organization of the phosphate backbone. Base pairing pattern is well maintained for all the ASO/RNA duplexes including the LNA/RNA control system with an optimum width of 11Å to 12Å. Because we have observed that the systems formed stable duplexes, we thus expect the base-pairing and base-stacking values to be close to the canonical reference values of standard nucleic acid duplexes [80]. Positive values of X-displacement indicate the helix axis to pass by the major groove whereas negative value indicates the helix to pass by the minor groove of the base pairs. In general, the X-displacement is negative for *A*-form duplexes like the RNAs or *A*-DNAs and Y-displacement is ~0 for both *A*-form and *B*-form duplexes. X-displacement in the modified ASO/RNA duplexes is negative. Rise values are ~2.5 Å for *A*-form duplexes and ~3.38Å for *B*-form duplexes. In our duplexes the rise values were concentrated in between ~1Å to ~2.5Å. Twist values are 32 for *A*-form duplexes 36 for *B*-form duplexes. In our duplexes the twist values are majorly below 34.

H-bonds play a critical role in stabilizing the secondary structure of DNA, RNA including base-pairing interactions and the overall helical conformation. Modifications to the bases or backbone can affect the number, strength, and geometry of H-bonds within the duplexes and their recognition by DNA-binding proteins or enzymes. Noting the importance of H-bonds, the inter-strand H-Bond distances, bond angles, bond residence frames for the ASO/RNA duplexes are calculated and studied. A % fraction of inter-strand H-Bonds formed throughout the simulation time is plotted in Figure 4.13. This figure is a simple representation of H-Bonds occurrence throughout the simulation trajectory from the data obtained from H-Bonds analysis. Results from the H-Bond analysis revealed that all the base pairs exhibited inter-strand H-Bond distances ~2.7Å to ~2.9 Å thus maintaining stable *Watson-crick* base pairing for the complete simulation trajectory. H-Bond parameters are in well agreement with the crystal data values corresponding to the *A*-form duplex structure of RNAs [80].

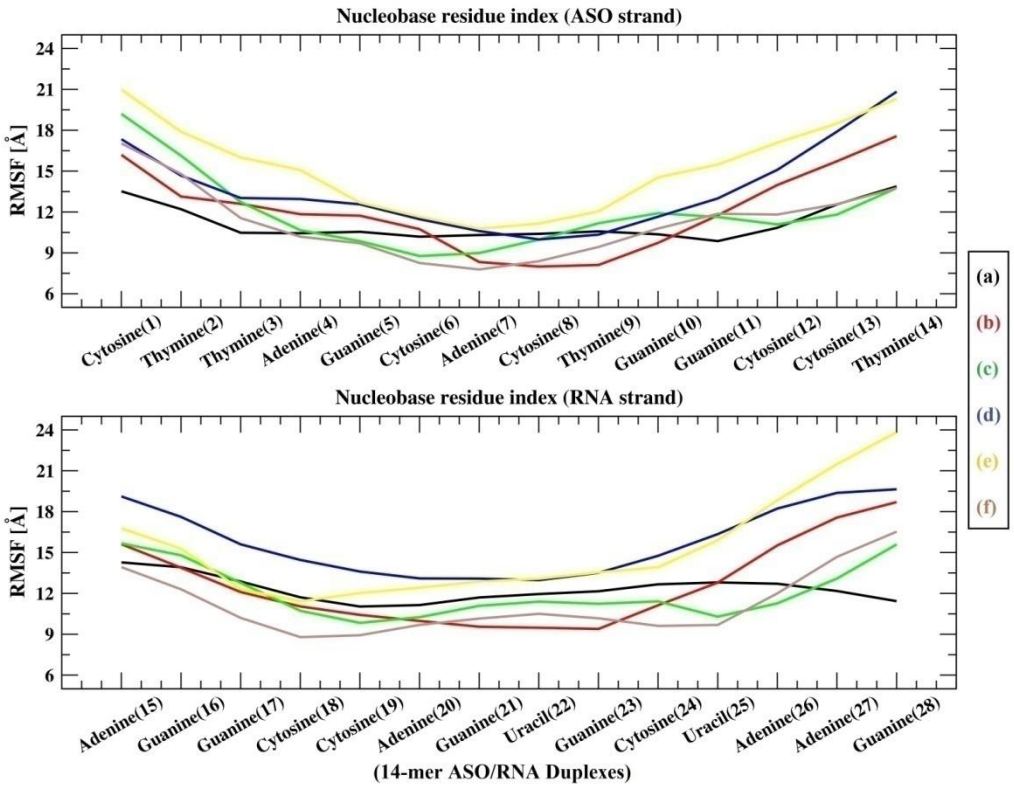

Figure 4.12: Backbone flexibility of monomer nucleotides of the 14-mer ASO/RNA duplexes (a) LNA/RNA (b) A1/RNA (c) A2/RNA (d) A3/RNA (e) A4/RNA and (f) A5/RNA for both the antisense and the sense strand for the entire simulation trajectory.

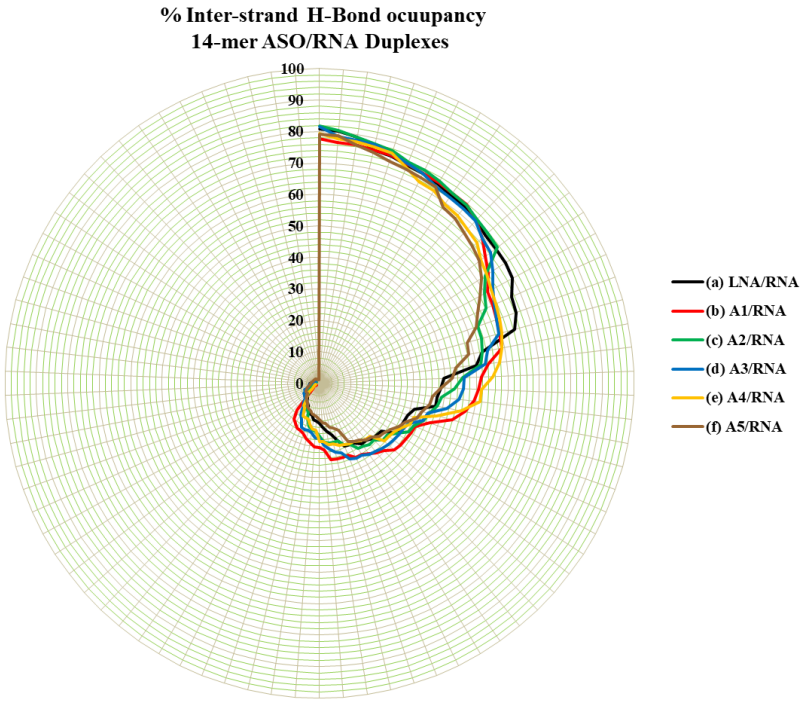

Figure 4.13: % occupancy of Inter-strand H-Bonds of the 14-mer ASO/RNA duplexes (a) LNA/RNA (b) A1/RNA (c) A2/RNA (d) A3/RNA (e) A4/RNA and (f) A5/RNA for the entire simulation trajectory.

4.3.2.5. SASA, MM-GBSA Binding Free Energy of the modified ASO/RNA duplexes

Solvent accessible surface area (SASA) and MM-GBSA binding free energy have always been considered as a decisive factor in research on protein folding and on drug-protein stability. Accordingly, the SASA and MM-GBSA free energy of the modified ASO/RNA duplexes can play an important role in understanding the solvation pattern including stability of the duplexes. Thus, solvation energies of all the six duplexes were evaluated by calculating their SASA values considering the entire simulation trajectory, enlisted in Table 4.4. It has already been reported of higher aqueous solubility of the LNA antisense modifications. Accordingly, results of SASA values revealed that solvation of all the duplexes wherein A2/RNA, A3/RNA, A4/RNA, A5/RNA were even higher than the LNA/RNA control system.

It has already been predicted from the monomer level studies that both purine and pyrimidine nucleobases bearing modifications A3, A4, A5 will be more inclined to donate as well as accept electrons compared to modifications A1, A2. Also, the molecular MO analysis predicted MO iso-surfaces for both purines and pyrimidines to be majorly distributed on the nucleobase region for modifications A1, A2 and in the bridging unit in-case of modifications A3, A4, A5. Results from the various global reactivity descriptors also suggested that modifications A3, A4, A5 will be more active in electron receiving and elimination processes during a chemical reaction and are expected to interact more with their surrounding environment including the cellular endonuclease RNase H compared to modifications A1, A2 irrespective of the type of nucleobase be it the purines or the pyrimidines. Relating the monomer conformational effects to the behaviour of these modifications at the oligomer level suggests the A3/RNA, A4/RNA, A5/RNA duplexes compared to the A1/RNA, A2/RNA duplexes to be highly available to the surrounding environment for various electron-exchange processes which may aid in the interaction with RNase H and solvent environment and thereby increase their antigene activity. Accordingly results from the SASA values revealed that solvation of A3/RNA, A4/RNA, A5/RNA duplexes were higher compared to LNA/RNA, A1/RNA, A2/RNA duplexes as their MO iso-surfaces were located on the bridging units which were highly available for solvation.

MM-GBSA is a post-simulation analysis method usually used to evaluate free energies of binding or to calculate absolute free energies of molecules in solution. We

have calculated the MM-GBSA free energy values of all the duplexes for the entire simulation trajectory, computed with the equation:

$$\Delta G_{binding} = G_{ASO/RNA} - G_{ASO} - G_{RNA}$$

Herein, the energies were calculated by considering the RNA strand as the target receptor, the ASO strand containing the modified nucleotides as binding ligands and ASO/RNA duplexes as the receptor-ligand complex molecule. The average MM-GBSA binding free energy values from the entire simulation trajectory are listed in Table 4.4. G_{RNA} energy values of the RNA strand has almost similar energy values for all the duplexes. The modified ASO strand on the other hand has different G_{ASO} energy values depending on the type of modifications. As seen in Table 4.4, although $G_{ASO/RNA}$ energy values of the duplexes were less yet A3/RNA, A4/RNA, A5/RNA duplexes has the nearest value compared to the control LNA/RNA system. On the other hand, although A1/RNA, A2/RNA, A3/RNA has lower $G_{ASO/RNA}$ energy values, the ΔG values of the same has the nearest value compared to the LNA/RNA control system. In fact, the A2/RNA, A3/RNA duplex has higher ΔG values compared to the LNA/RNA control system. Thus, the MM-GBSA binding energies of the modified ASO/RNA duplexes containing the proposed LNA analogue antisense modifications estimated for the entire simulation trajectory were predicted to be equally stable as the LNA/RNA control system.

Table 4.4: SASA and MM-GBSA free energies of the 14-mer ASO/RNA duplexes (a) LNA/RNA (b) A1/RNA (c) A2/RNA (d) A3/RNA (e) A4/RNA and (f) A5/RNA for the entire simulation trajectory.

ASO/RNA Duplexes	SASA (Å^2)	MM-GBSA (kcal/mol)			
		$G_{ASO/RNA}$	G_{RNA}	G_{ASO}	ΔG
(a) LNA/RNA	5966.939	-4075.61	-1876.88	-2084.73	-113.98
(b) A1/RNA	5841.794	-3474.70	-1274.21	-2088.58	-111.90
(c) A2/RNA	6224.247	-3571.79	-1360.86	-2095.24	-115.68
(d) A3/RNA	6396.581	-3705.86	-1499.91	-2091.72	-114.21
(e) A4/RNA	6330.429	-3848.07	-1657.60	-2084.94	-105.52
(f) A5/RNA	6314.375	-3928.79	-1724.63	-2097.86	-106.29

4.4. Summary

The present work focuses to perform a detailed quantum chemical study of five novel LNA analogue antisense alterations (A1, A2, A3, A4, A5) and establishing each with the five standard nucleic acids Adenine(A), Guanine(G), Cytosine(C), Thymine(T) and Uracil(U), respectively at the monomer level using DFT methods and to relate the conformational effects induced by these alterations at the oligomer level by using MD simulations studies. Accordingly, we have studied the structural, electronic properties and quantum chemical parameters of the proposed antisense modifications at the monomer level. Oligomer level hybrid duplex stability containing the modifications is described performing a detailed MD simulation study by incorporating the modifications onto 14-mer ASO/RNA duplex systems.

According to the monomer level investigation, there is no disturbance in the *N-type* sugar puckering due to infusion of the proposed alterations. Also, the relative sugar-base orientation existed in an *anti*-conformation which can increase the strength of base pairing and base stacking interactions preferring RNA-mimicking conformations. Monomer nucleotides with modifications A3, A4, A5 are predicted to be better electron donors as well as better electron acceptors compared to A1, A2 for both the purine and pyrimidine nucleobases. HOMO-LUMO isosurfaces of A1, A2 are majorly distributed on the nucleobase region whereas for A3, A4, A5 are well distributed in the modified bridging unit for both the purine and pyrimidine nucleobases. In A1, A2 the MO isosurfaces being embedded in the nucleobase region might decrease their possibility of interactions with RNase H and solvent environment. On the contrary in A3, A4, A5 the MO isosurfaces being well distributed in the modified bridging unit will be highly available to the surrounding environment for various electron-exchange processes which may aid in the interaction with RNase H and solvent environment and thereby increase their antigene activity.

Further, derivation of the global reactivity descriptors global hardness (η), global softness (S), chemical potential (μ) and electrophilicity (ω) of the monomer nucleotides has helped in understanding dependency of their electronic properties with varying structural modifications. Global hardness and softness suggest that modifications A3, A4, A5 will be more active in electron receiving and elimination processes or softer during a chemical reaction compared to modifications A1, A2 irrespective of the type of nucleobase be it the purines or the pyrimidines. Chemical potential results suggests that

A1, A2, A5 have more negative and A3, A4 have less negative chemical potential values for the purines; and A1, A2, have more negative and A3, A4, A5 have less negative chemical potential values for the pyrimidines. Electrophilicity results suggest that A3, A4 are less electrophilic while A1, A2, A5 are more electrophilic irrespective of the type of nucleobase be it the purines or the pyrimidines. This is an implication of A3, A4 having high lying E_{HOMO} which will accept electrons less easily, rather will donate more easily and hence less electrophilic, compared to A1, A2, A5 having low lying E_{HOMO} which will donate electrons less easily, rather will accept more easily and hence more electrophilic. Overall, modifications A3, A4 have less negative chemical potential and are less electrophilic compared to modifications A1, A2, A5 for both the purine and pyrimidine nucleobases. Such small changes in the values of the descriptors may be useful in capturing differences between the proposed antisense modifications at the monomer level which may contribute to understanding the behavior of these modifications at the oligomer level.

According to the oligomer level investigation, the 2′carbon and 4′carbon bridges in the modified ASO/RNA duplexes were located towards the edge of the minor groove maintaining stable helical structures. The oligomer duplex structure, sugar-pucker, N-glycosidic torsion angle distributions, backbone conformation, base-pairing, base-stacking, H-bond distances, base-pair distances all were in accordance, trying to adopt right-handed *A-form* helix preferring RNA-mimicking *A-form* geometries which can increase the strength of base pairing and base-stacking interactions during duplex formation. The duplexes exhibited stable RMSD's compared to the LNA and MOE modified hybrids reported in literature. Wherein structural studies reported low flexibility of fully modified LNA/RNA duplexes, the modified duplexes in our case exhibited higher flexibility compared to the LNA/RNA duplexes suggesting these modifications to induce higher flexibility compared to the parent LNA modification, the very reason for considering fully modified duplexes in the present study.

Monomer level studies clearly predicted MO surfaces to be majorly distributed on the nucleobase region in A1, A2 and in the bridging unit in A3, A4, A5. Results from the various global reactivity descriptors also suggested that compared to A1, A2 modifications A3, A4, A5 will be more active in electron receiving and elimination processes during a chemical reaction and are expected to interact more with their surrounding environment including the cellular endonuclease RNase H. Relating the

monomer conformational effects to the behavior of these modifications at the oligomer level suggests A3/RNA, A4/RNA, A5/RNA duplexes compared to A1/RNA, A2/RNA duplexes to be highly available to the surrounding environment for various electron-exchange processes which may aid in the interaction with RNase H and solvent environment and thereby increase their antigene activity. Accordingly, solvation of A3/RNA, A4/RNA, A5/RNA duplexes were higher compared to LNA/RNA, A1/RNA, A2/RNA duplexes as their MO iso-surfaces located on the bridging units were highly available for solvation. This study has resulted in a successful archetype for creating advantageous nucleic acid modifications tailored for particular needs in designing novel antisense modifications which may overcome the drawbacks and improve the pharmacokinetics of existing LNA antisense modifications.

Bibliography

[1] Chan, J. H., Lim, S., and Wong, W. F. Antisense oligonucleotides: from design to therapeutic application. *Clinical and Experimental Pharmacology and Physiology*, 33(5-6):533-540, 2006.

[2] Crooke, S. T. ed. Antisense drug technology: principles, strategies, and applications. CRC press, 2007.

[3] Bennett, C. F., and Swayze, E. E. RNA targeting therapeutics: molecular mechanisms of antisense oligonucleotides as a therapeutic platform. *Annual Review of Pharmacology*, 50:259-293, 2010.

[4] Zamaratski, E., Pradeepkumar, P. I., and Chattopadhyaya, J. A critical survey of the structure-function of the antisense oligo/RNA hetero duplex as substrate for RNase H. *Journal of Biochemical and Biophysical Methods*, 48(3):189-208, 2001.

[5] Nowotny, M., Gaidamakov, S. A., Ghirlando, R., Cerritelli, S. M., Crouch, R. J., and Yang, W. Structure of human RNase H1 complexed with an RNA/DNA hybrid: insight into HIV reverse transcription. *Molecular Cell*, 28(2):264-276, 2007.

[6] Herbert, C., Dzowo, Y. K., Urban, A., Kiggins, C. N., and Resendiz, M. J. Reactivity and specificity of RNase T1, RNase A, and RNase H toward oligonucleotides of RNA containing 8-Oxo-7, 8-dihydroguanosine. *Biochemistry*, 57(20):2971-2983, 2018.

[7] Kiełpiński, Ł. J., Hagedorn, P. H., Lindow, M., and Vinther, J. RNase H sequence preferences influence antisense oligonucleotide efficiency. *Nucleic Acids Research*, 45(22):12932-12944, 2017.

[8] Hagedorn, P. H., Pontoppidan, M., Bisgaard, T. S., Berrera, M., Dieckmann, A., Ebeling, M., Møller, M. R., Hudlebusch, H., Jensen, M. L., Hansen, H. F., and Koch, T. Identifying and avoiding off-target effects of RNase H-dependent antisense oligonucleotides in mice. *Nucleic Acids Research,* 46(11):5366-5380, 2018.

[9] Campbell, J. M., Bacon, T. A., and Wickstrom, E. Oligodeoxynucleoside phosphorothioate stability in subcellular extracts, culture media, sera and cerebrospinal fluid. *Journal of Biochemical and Biophysical Methods***,** 20(3):259-267, 1990.

[10] Zhang, R., Diasio, R. B., Lu, Z., Liu, T., Jiang, Z., Galbraith, W. M., and Agrawal, S. Pharmacokinetics and tissue distribution in rats of an oligodeoxynucleotide phosphorothioate (GEM 91) developed as a therapeutic agent for human immunodeficiency virus type-1. *Biochemical Pharmacology,* 49(7):929-939, 1995.

[11] Agrawal, S., Goodchild, J., Civeira, M., Sarin, P. S., and Zamecnik, P. C. Phosphoramidate, phosphorothioate, and methylphosphonate analogs of oligodeoxynucleotide: inhibitors of replication of human immunodeficiency virus. *Nucleosides Nucleotides Nucleic Acids,* 8(5-6):819-823, 1989.

[12] Iwamoto, N., Butler, D. C., Svrzikapa, N., Mohapatra, S., Zlatev, I., Sah, D. W., Standley, S. M., Lu, G., Apponi, L. H., Frank-Kamenetsky, M., and Zhang, J. J. Control of phosphorothioate stereochemistry substantially increases the efficacy of antisense oligonucleotides. *Nature Biotechnology,* 35(9):845-851, 2017.

[13] Shen, W., De Hoyos, C. L., Migawa, M. T., Vickers, T. A., Sun, H., Low, A., Bell, T. A., Rahdar, M., Mukhopadhyay, S., Hart, C. E., and Bell, M. Chemical modification of PS-ASO therapeutics reduces cellular protein-binding and improves the therapeutic index. *Nature Biotechnology,* 37(6):640-650, 2019.

[14] Manoharan, M. 2′-Carbohydrate modifications in antisense oligonucleotide therapy: importance of conformation, configuration and conjugation. *Biochimica et Biophysica Acta (BBA) - Gene Structure and Expression,* 1489(1):117-130, 1999.

[15] Herdewijn, P. Conformationally restricted carbohydrate-modified nucleic acids and antisense technology. *Biochimica et Biophysica Acta (BBA) - Gene Structure and Expression*, 1489(1):167-179, 1999.

[16] Finn, P. J., Gibson, N. J., Fallon, R., Hamilton, A., and Brown, T. Synthesis and properties of DNA-PNA chimeric oligomers. *Nucleic Acids Research,* 24(17):3357-3363, 1996.

[17] Rosie, Z. Y., Kim, T. W., Hong, A., Watanabe, T. A., Gaus, H. J., and Geary, R .S. Cross-species pharmacokinetic comparison from mouse to man of a second-generation antisense oligonucleotide, ISIS 301012, targeting human apolipoprotein B-100. *Drug Metabolism and Disposition*, 35(3):460-468, 2007.

[18] Geary, R. S., Wancewicz, E., Matson, J., Pearce, M., Siwkowski, A., Swayze, E., and Bennett, F. Effect of dose and plasma concentration on liver uptake and pharmacologic activity of a 2′-methoxyethyl modified chimeric antisense oligonucleotide targeting PTEN. *Biochemical Pharmacology*, 78(3):284-291, 2009.

[19] Post, N., Yu, R., Greenlee, S., Gaus, H., Hurh, E., Matson, J., and Wang, Y. Metabolism and disposition of volanesorsen, a 2′-O-(2 methoxyethyl) antisense oligonucleotide, across species. *Drug Metabolism and Disposition*, 47(10):1164-1173, 2019.

[20] Kurreck, J. Antisense technologies: improvement through novel chemical modifications. *European Journal of Biochemistry*, 270(8):1628-1644, 2003.

[21] Moss, K. H., Popova, P., Hadrup, S. R., Astakhova, K., and Taskova, M. Lipid nanoparticles for delivery of therapeutic RNA oligonucleotides. *Molecular Pharmaceutics*, 16(6):2265-2277, 2019.

[22] Gheibi-Hayat, S. M., and Jamialahmadi, K. Antisense Oligonucleotide (AS-ODN) Technology: Principle, Mechanism and Challenges. *Biotechnology and Applied Biochemistry*, 68(5):1086-1094, 2021.

[23] Vitravene Study Group, A randomized controlled clinical trial of intravitreous fomivirsen for treatment of newly diagnosed peripheral cytomegalovirus retinitis in patients with AIDS. *American Journal of Ophthalmology*, 133(4):467-474, 2002.

[24] Le Calvez, H., Yu, M., and Fang, F. Biochemical prevention and treatment of viral infections–A new paradigm in medicine for infectious diseases. *Virology Journal*, 1:1-6, 2004.

[25] Stein, C. A., and Castanotto, D. FDA-approved oligonucleotide therapies in 2017. *Molecular Therapy*, 25(5):1069-1075, 2017.

[26] Silva, A. C., Lobo, D. D., Martins, I. M., Lopes, S. M., Henriques, C., Duarte, S. P., Dodart, J. C., Nobre, R. J., and Pereira de Almeida, L. Antisense oligonucleotide therapeutics in neurodegenerative diseases: the case of polyglutamine disorders. *Brain*, 143(2):407-429, 2020.

[27] Takei, Y., Kadomatsu, K., Yuzawa, Y., Matsuo, S., and Muramatsu, T. A small interfering RNA targeting vascular endothelial growth factor as cancer therapeutics. *Cancer Research*, 64(10):3365-3370, 2004.

[28] Gong, M., Lu, Z., Fang, G., Bi, J., and Xue, X. A small interfering RNA targeting osteopontin as gastric cancer therapeutics. *Cancer Letters*, 272(1):148-159, 2008.

[29] Singh, S. K., Koshkin, A. A., Wengel, J., and Nielsen, P. LNA (locked nucleic acids): synthesis and high-affinity nucleic acid recognition. *Chemical Communications*, (4):455-456, 1998.

[30] Abdur Rahman, S. M., Seki, S., Obika, S., Yoshikawa, H., Miyashita, K., and Imanishi, T. Design, Synthesis, and Properties of 2 ‘,4 ‘-BNA^{NC}: A Bridged Nucleic Acid Analogue. *Journal of American Chemical Society*, 130(14):4886-4896, 2008.

[31] Shrestha, A. R., Kotobuki, Y., Hari, Y., and Obika, S. Guanidine bridged nucleic acid (GuNA): an effect of a cationic bridged nucleic acid on DNA binding affinity. *Chemical Communications*, 50(5):575-577, 2014.

[32] Langner, H. K., Jastrzebska, K., and Caruthers, M. H. Synthesis and characterization of thiophosphoramidate morpholino oligonucleotides and chimeras. *Journal of American Chemical Society*, 142(38):16240-16253, 2020.

[33] Fluiter, K., ten Asbroek, A. L., de Wissel, M. B., Jakobs, M. E., Wissenbach, M., Olsson, H., Olsen, O., Oerum, H., and Baas, F. In vivo tumor growth inhibition, and biodistribution studies of locked nucleic acid (LNA) antisense oligonucleotides. *Nucleic Acids Research*, 31(3):953-962, 2003.

[34] Darfeuille, F., Hansen, J. B., Orum, H., Primo, C. D., and Toulmé, J. J. LNA/DNA chimeric oligomers mimic RNA aptamers targeted to the TAR RNA element of HIV-1. *Nucleic Acids Research*, 32(10):3101-3107, 2004.

[35] Laxton, C., Brady, K., Moschos, S., Turnpenny, P., Rawal, J., Pryde, D. C., Sidders, B., Corbau, R., Pickford, C., and Murray, E. J. Selection, optimization, and pharmacokinetic properties of a novel, potent antiviral locked nucleic acid-based antisense oligomer targeting hepatitis C virus internal ribosome entry site. *Antimicrobial Agents and Chemotherapy*, 55(7):3105-3114, 2011.

[36] Swayze, E. E., Siwkowski, A. M., Wancewicz, E. V., Migawa, M. T., Wyrzykiewicz, T. K., Hung, G., Monia, B. P., and Bennett, A. C. F. Antisense oligonucleotides containing locked nucleic acid improve potency but cause significant hepatotoxicity in animals. *Nucleic Acids Research*, 35(2):687-700, 2007.

[37] Seth, P. P., Siwkowski, A., Allerson, C. R., Vasquez, G., Lee, S., Prakash, T. P., Wancewicz, E. V., Witchell, D., and Swayze, E. E. Short antisense oligonucleotides with novel 2′− 4′ conformationaly restricted nucleoside analogues show improved potency without increased toxicity in animals. *Journal of Medicinal Chemistry*, 52(1):10-13, 2009.

[38] Seth, P. P., Vasquez, G., Allerson, C. A., Berdeja, A., Gaus, H., Kinberger, G. A., Prakash, T. P., Migawa, M. T., Bhat, B., and Swayze, E. E. Synthesis and biophysical evaluation of 2′, 4′-constrained 2′ O-methoxyethyl and 2′, 4′-constrained 2′ O-ethyl nucleic acid analogues. *The Journal of Organic Chemistry*, 75(5):1569-1581, 2010.

[39] Prakash, T. P., Siwkowski, A., Allerson, C. R., Migawa, M. T., Lee, S., Gaus, H. J., Black, C., Seth, P. P., Swayze, E. E., and Bhat, B. Antisense oligonucleotides containing conformationally constrained 2′, 4′-(N-methoxy) aminomethylene and 2′, 4′-aminooxymethylene and 2′-O, 4′-C-aminomethylene bridged nucleoside analogues show improved potency in animal models. *Journal of Medicinal Chemistry*, 53(4):1636-1650, 2010.

[40] Yamamoto, T., Yasuhara, H., Wada, F., Harada-Shiba, M., Imanishi, T., and Obika, S. Superior silencing by 2′,4′-BNA^{NC}-based short antisense oligonucleotides compared to 2′,4′-BNA/LNA-based apolipoprotein B antisense inhibitors. *Journal of Nucleic Acids*, 2012.

[41] Natsume, T., Ishikawa, Y., Dedachi, K., Tsukamoto, T., and Kurita, N. DFT study of the electronic properties of DNA–DNA and PNA–DNA double strands. *International Journal of Quantum Chemistry*, 106(15):3278-3287, 2006.

[42] Uppuladinne, M. V., Jani, V., Sonavane, U. B., and Joshi, R. R. Quantum chemical studies of novel 2′-4′ conformationally restricted antisense monomers. *International Journal of Quantum Chemistry*, 113(23):2523-2533, 2013.

[43] Bhai, S., and Ganguly, B. Role of backbones on the interaction of metal ions with deoxyribonucleic acid and peptide nucleic acid: A DFT study. *Journal of Molecular Graphics*, 93:107445, 2019.

[44] Uppuladinne, M. V., Sonavane, U. B., Deka, R. C., and Joshi, R. R. Structural insight into antisense gapmer-RNA oligomer duplexes through molecular dynamics simulations. *Journal of Biomolecular Structure and Dynamics*, 37(11):2823-2836, 2019.

[45] Galindo-Murillo, R., Cohen, J. S., and Akabayov, B. Molecular dynamics simulations of acyclic analogs of nucleic acids for antisense inhibition. *Molecular Therapy - Nucleic Acids*, 23:527-535, 2021.

[46] Hansen, H. F., Albaek, N., Hansen, B. R., Shim, I., Bohr, H., and Koch, T. In vivo uptake of antisense oligonucleotide drugs predicted by ab initio quantum mechanical calculations. *Scientific Reports*, 11(1):1-13, 2021.

[47] Uppuladinne, M. V., Dowerah, D., Sonavane, U. B., Ray, S. K., Deka, R. C., and Joshi, R. R. Structural Insight into Locked Nucleic Acid based Novel Antisense Modifications: A DFT calculations at monomer and MD simulations at oligomer level. *Journal of Molecular Graphics*, 107:107945, 2021.

[48] BIOVIA, DassaultSystèmes, [Discovery Studio], [Client version 19.1.0], San Diego: DassaultSystèmes, 2019.

[49] Frisch, M. J., Trucks, G.W., Schlegel, H. B., Scuseria, G. E., Robb, M., Cheeseman, J. R., Scalmani, G., Barone, V., Mennucci, B., Petersson, G. A., Nakatsuji, H. et al. *Gaussian 09* (Revision D.01); Gaussian. Inc.: Wallingford CT, 2009.

[50] Hehre, W. J., Ditchfield, R., and Pople, J. A. Self—consistent molecular orbital methods. XII. Further extensions of Gaussian—type basis sets for use in molecular orbital studies of organic molecules. *The Journal of Chemical Physics*, 56(5):2257-2261, 1972.

[51] Hariharan, P. C., and Pople, J. A. The influence of polarization functions on molecular orbital hydrogenation energies. *Theoretica Chimica Acta*, 28:213-222, 1973.

[52] Zhao, Y., and Truhlar, D. G. The M06 suite of density functionals for main group thermochemistry, thermochemical kinetics, noncovalent interactions, excited states, and transition elements: two new functionals and systematic testing of four M06-class functionals and 12 other functionals. *Theoretical Chemistry Accounts*, 120:215-241, 2008.

[53] Wang, Y., Verma, P., Jin, X., Truhlar, D. G., and He, X. Revised M06 density functional for main-group and transition-metal chemistry. *Proceedings of the National Academy of Sciences of the United States of America*, 115(41):10257-10262, 2018.

[54] Takano, Y., and Houk, K. N. Benchmarking the conductor-like polarizable continuum model (CPCM) for aqueous solvation free energies of neutral and ionic organic molecules. *Journal of Chemical Theory and Computation*, 1(1):70-77, 2005.

[55] Lu, T., and Chen, F. Multiwfn: a multifunctional wavefunction analyzer. *Journal of Computational Chemistry*, 33(5):580-592, 2012.

[56] Parr, R. G., and Yang, W. Density functional approach to the frontier-electron theory of chemical reactivity. *Journal of American Chemical Society*, 106(14):4049-4050, 1984.

[57] Luo, J., Xue, Z. Q., Liu, W. M., Wu, J. L., and Yang, Z. Q. Koopmans' theorem for large molecular systems within density functional theory. *Journal of Physical Chemistry A*, 110(43):12005-12009, 2006.

[58] Vijayaraj, R., Subramanian, V., and Chattaraj, P. K. Comparison of global reactivity descriptors calculated using various density functionals: a QSAR perspective. *Journal of Chemical Theory and Computation*, 5(10):2744-2753, 2009.

[59] Cornell, W. D., Cieplak, P., Bayly, C. I., Gould, I. R., Merz, K. M., Ferguson, D. M., Spellmeyer, D. C., Fox, T., Caldwell, J. W., and Kollman, P. A. A second generation force field for the simulation of proteins, nucleic acids, and organic molecules. *Journal of American Chemical Society*, 117(19):5179-5197, 1995.

[60] Pérez, A., Marchán, I., Svozil, D., Sponer, J., Cheatham III, T. E., Laughton, C. A., and Orozco, M. Refinement of the AMBER force field for nucleic acids: improving the description of α/γ conformers. *Biophysical Journal*, 92(11):3817-3829, 2007.

[61] Case, D., Ben-Shalom, I., Brozell, S., Cerutti, D., Cheatham, T., III, V. C., Darden, T., Duke, R., Ghoreishi, D., Gilson, M. et al. *AMBER*, University of California: San Francisco, 2018.

[62] Jorgensen, W. L., Chandrasekhar, J., Madura, J. D., Impey, R. W., and Klein, M. L. Comparison of simple potential functions for simulating liquid water. *The Journal of Chemical Physics*, 79(2):926-935, 1983.

[63] Machireddy, B., Kalra, G., Jonnalagadda, S., Ramanujachary, K., and Wu, C. Probing the binding pathway of BRACO19 to a parallel-stranded human telomeric G-quadruplex using molecular dynamics binding simulation with AMBER DNA OL15 and ligand GAFF2 force fields. *Journal of Chemical Information and Modeling*, 57(11):2846-2864, 2017.

[64] Zhao, J., Kennedy, S. D., and Turner, D. H. Nuclear Magnetic Resonance Spectra and AMBER OL3 and ROC-RNA Simulations of UCUCGU Reveal Force Field Strengths and Weaknesses for Single-Stranded RNA. *Journal of Chemical Theory and Computation*, 18(2):1241-1254, 2022.

[65] Cheatham, T. I., Miller, J. L.; Fox, T., Darden, T. A., and Kollman, P. A. Molecular dynamics simulations on solvated biomolecular systems: the particle mesh Ewald method leads to stable trajectories of DNA, RNA, and proteins. *Journal of American Chemical Society*, 117(14):4193-4194, 1995.

[66] Miyamoto, S., and Kollman, P. A. Settle: An analytical version of the SHAKE and RATTLE algorithm for rigid water models. *Journal of Computational Chemistry*, 13(8):952-962, 1992.

[67] Roe, D. R., and Cheatham III, T. E. PTRAJ and CPPTRAJ: software for processing and analysis of molecular dynamics trajectory data. *Journal of Chemical Theory and Computation*, 9(7):3084-3095, 2013.

[68] Humphrey, W., Dalke, A., and Schulten, K. VMD: visual molecular dynamics. *Journal of Molecular Graphics*, 14(1):33-38, 1996.

[69] Xu, L., Sun, H., Li, Y., Wang, J., and Hou, T. Assessing the performance of MM/PBSA and MM/GBSA methods. 3. The impact of force fields and ligand charge models. *The Journal of Physical Chemistry B*, 117(28):8408-8421, 2013.

[70] Golyshev, V. M., Pyshnyi, D. V., and Lomzov, A. A. Calculation of Energy for RNA/RNA and DNA/RNA Duplex Formation by Molecular Dynamics Simulation. *Molecular Biology*, 55(6):927-940, 2021.

[71] Braasch, D. A., and Corey, D. R. Locked nucleic acid (LNA): fine-tuning the recognition of DNA and RNA. *ACS Chemical Biology*, 8(1):1-7, 2001.

[72] Hanessian, S., Schroeder, B. R., Giacometti, R. D., Merner, B. L., Østergaard, M., Swayze, E. E., and Seth, P. P. Structure-Based Design of a Highly Constrained Nucleic Acid Analogue: Improved Duplex Stabilization by Restricting Sugar Pucker and Torsion Angle γ. *Angewandte Chemie*, 124:11404-11407, 2012.

[73] Levitt, M., and Warshel, A. Extreme conformational flexibility of the furanose ring in DNA and RNA. *Journal of American Chemical Society*, 100(9):2607-2613, 1978.

[74] Heinemann, U., and Roske, Y. Symmetry in nucleic-acid double helices. *Symmetry*, 12(5):737, 2020.

[75] Ho, P. S., and Carter, M. DNA structure: Alphabet soup for the cellular soul. In DNA Replication-Current Advances. *IntechOpen,* 2011.

[76] Xia, Z., Bell, D. R., Shi, Y., and Ren, P. RNA 3D structure prediction by using a coarse-grained model and experimental data. *The Journal of Physical Chemistry B,* 117(11):3135-3144, 2013.

[77] Sponer, J., Zgarbová, M., Jurecka, P., Riley, K. E., Sponer, J. E., and Hobza, P. Reference quantum chemical calculations on RNA base pairs directly involving the 2′-OH group of ribose. *Journal of Chemical Theory and Computation,* 5(4):1166-1179, 2009.

[78] Butcher, S. E., and Pyle, A. M. The molecular interactions that stabilize RNA tertiary structure: RNA motifs, patterns, and networks. *Accounts of Chemical Research,* 44(12):1302-1311, 2011.

[79] Yakovchuk, P., Protozanova, E., and Frank-Kamenetskii, M. D. Base-stacking and base-pairing contributions into thermal stability of the DNA double helix. *Nucleic Acids Research,* 34(2):564-574, 2006.

[80] Parker, T. M., Hohenstein, E. G., Parrish, R. M., Hud, N. V., and Sherrill, C. D. Quantum-mechanical analysis of the energetic contributions to π stacking in nucleic acids versus rise, twist, and slide. *Journal of American Chemical Society,* 135(4):1306-1316, 2013.